

# Searching for chameleon-like scalar fields with the ammonia method<sup>\*</sup>

S. A. Levshakov<sup>1,2</sup>, P. Molaro<sup>1</sup>, A. V. Lapinov<sup>3</sup>, D. Reimers<sup>4</sup>, C. Henkel<sup>5</sup>, and T. Sakai<sup>6</sup>

<sup>1</sup> INAF-Osservatorio Astronomico di Trieste, Via G. B. Tiepolo 11, 34131 Trieste, Italy

<sup>2</sup> Ioffe Physical-Technical Institute, Polytekhnicheskaya Str. 26, 194021 St. Petersburg, Russia  
e-mail: lev@astro.ioffe.rssi.ru

<sup>3</sup> Institute for Applied Physics, Uljanov Str. 46, 603950 Nizhny Novgorod, Russia

<sup>4</sup> Hamburger Sternwarte, Universität Hamburg, Gojenbergsweg 112, D-21029 Hamburg, Germany

<sup>5</sup> Max-Planck-Institut für Radioastronomie, Auf dem Hügel 69, D-53121 Bonn, Germany

<sup>6</sup> Institute of Astronomy, The University of Tokyo, Osawa, Mitaka, Tokyo 181-0015, Japan

Received 00 ; Accepted 00

## ABSTRACT

**Aims.** We probe the dependence of the electron-to-proton mass ratio,  $\mu = m_e/m_p$ , on the ambient matter density by means of radio astronomical observations.

**Methods.** The ammonia method, which has been proposed to explore the electron-to-proton mass ratio, is applied to nearby dark clouds in the Milky Way. This ratio, which is measured in different physical environments of high (terrestrial) and low (interstellar) densities of baryonic matter is supposed to vary in chameleon-like scalar field models, which predict strong dependences of both masses and coupling constant on the local matter density. High resolution spectral observations of molecular cores in lines of  $\text{NH}_3$  ( $J, K$ ) = (1, 1),  $\text{HC}_3\text{N}$   $J = 2 - 1$ , and  $\text{N}_2\text{H}^+$   $J = 1 - 0$  were performed at three radio telescopes to measure the radial velocity offsets,  $\Delta V \equiv V_{\text{rot}} - V_{\text{inv}}$ , between the inversion transition of  $\text{NH}_3$  (1,1) and the rotational transitions of other molecules with different sensitivities to the parameter  $\Delta\mu/\mu \equiv (\mu_{\text{obs}} - \mu_{\text{lab}})/\mu_{\text{lab}}$ .

**Results.** The measured values of  $\Delta V$  exhibit a statistically significant velocity offset of  $23 \pm 4_{\text{stat}} \pm 3_{\text{sys}}$  m s<sup>-1</sup>. When interpreted in terms of the electron-to-proton mass ratio variation, this infers that  $\Delta\mu/\mu = (2.2 \pm 0.4_{\text{stat}} \pm 0.3_{\text{sys}}) \times 10^{-8}$ . If only a conservative upper bound is considered, then the maximum offset between ammonia and the other molecules is  $|\Delta V| \leq 30$  m s<sup>-1</sup>. This provides the most accurate reference point at  $z = 0$  for  $\Delta\mu/\mu$  of  $|\Delta\mu/\mu| \leq 3 \times 10^{-8}$ .

**Key words.** Line: profiles – ISM: molecules – Radio lines: ISM – Techniques: radial velocities

## 1. Introduction

Testing the variability of dimensionless physical constants is an important topic in contemporary laboratory and astrophysical experiments. The physical constants are not supposed to vary in the Standard Model (SM) of particle physics but do vary quite naturally in grand unification theories, multidimensional theories, and whenever there is a coupling between light scalar fields and baryonic matter. In particular, light scalar fields have been widely discussed in the context of dark energy, since they provide negative pressure that may be responsible for the cosmic acceleration detected at low redshifts,  $z < 1$  (Caldwell et al. 1998; Peebles & Rata 2003). If this scalar field does exist, then a question arises: why has it not been detected in local tests of the equivalence principle or fifth force searches? A solution was suggested using the so-called ‘chameleon’ models (Khouri & Weltman 2004; Brax et al. 2004; Mota & Shaw 2007). These models assume that a light scalar field acquires both an effective potential and effective mass be-

cause of its coupling to matter that strongly depends on the ambient matter density. In this way, this scalar field may evade local tests of the equivalence principle and fifth force experiments since the range of the scalar-mediated fifth force for the terrestrial matter densities is too small to be detected. This is not the case for space-based tests, where the matter density is considerably lower, an effective mass of the scalar field is negligible, and an effective range for the scalar-mediated force is large. The present paper deals with one such astronomical test based on spectral observations of molecular clouds in the Milky Way disk. Additional tests employing polarization of the light from the stars and a modification of the Sunyaev-Zel’dovich effect in the cosmic microwave background due to a coupling between a chameleon-like scalar field and photons are described, respectively, in Burrage et al. (2009) and Davis et al. (2009).

Astronomical spectroscopy can probe the physical constants that describe atomic and molecular discrete spectra: the fine-structure constant,  $\alpha = e^2/(\hbar c)$ , and the electron-to-proton mass ratio,  $\mu = m_e/m_p$ . In GUTs, these constants mediate the strength of fundamental forces:  $\alpha$  is the coupling constant of the electromagnetic interaction,  $m_e$  is related to the vacuum expectation value of the Higgs field, namely to the scale of the weak nuclear force, and  $m_p$  is

\* Based on observations obtained with the Medicina 32-m telescope operated by INAF – Istituto di Radioastronomia, the 100-m telescope of the Max-Planck Institut für Radioastronomie at Effelsberg, and the Nobeyama Radio Observatory 45-m telescope of the National Astronomical Observatory of Japan.

proportional to the quantum chromodynamics scale. We note that the predicted variabilities of the fine-structure constant and the electron-to-proton mass ratio are not independent and that the variations in  $\mu$  may exceed those of  $\alpha$  (Calmet & Fritzsche 2002; Langacker et al. 2002; Dine et al. 2003; Flambaum et al. 2004). Thus, a hypothetical variation in  $\mu$  is expected to be easier to detect than that in  $\alpha$ .

Despite many efforts, the variability in  $\alpha$  and  $\mu$  has never been detected. Data obtained from high precision frequency measurements in laboratory experiments with atomic clocks and from astronomical observations provide only upper limits. For example, laboratory experiments have delivered the following results: fractional temporal variations in  $\mu$  are restricted to a level of  $\dot{\mu}/\mu = (3.8 \pm 5.6) \times 10^{-14} \text{ yr}^{-1}$  (Shelkovnikov et al. 2008), and  $\dot{\mu}/\mu = (1.6 \pm 1.7) \times 10^{-15} \text{ yr}^{-1}$  (Blatt et al. 2008), whereas the current level for  $\alpha$  is  $\dot{\alpha}/\alpha = (-1.6 \pm 2.3) \times 10^{-17} \text{ yr}^{-1}$  (Rosenband et al. 2008). Here  $\Delta\mu$  and  $\Delta\alpha$  are the relative changes between the values measured at two different epochs.

The most stringent upper limits to  $\Delta\alpha/\alpha$  and  $\Delta\mu/\mu$  obtained from astronomical observations of extragalactic objects are restricted by a few units of ppm (1ppm =  $10^{-6}$ ). Here  $\Delta\alpha/\alpha = (\alpha' - \alpha)/\alpha$ , where  $\alpha, \alpha'$  denote the values of the fine-structure constant in the laboratory and the specific absorption/emission line system of a Galactic or extragalactic object (the same definition is applied to  $\Delta\mu/\mu$ ). However, there are claims of a variability in both  $\alpha$  and  $\mu$  at the  $5\sigma$  and  $4\sigma$  confidence levels, respectively, although they are in contrast to other null results and the whole issue is highly controversial. The current observational status is the following.

From the measurements of the relative radial velocity shifts of different absorption lines (e.g., Mg II, Si II, Fe II, Zn II) of 143 QSO absorption systems obtained with the Keck/HIRES in the redshift range  $0.2 < z < 4.2$ , Murphy et al. (2004) claimed that  $\Delta\alpha/\alpha = -5.7 \pm 1.1$  ppm. On the other hand, Chand et al. (2004) using VLT/UVES spectra of bright QSOs analyzed 23 absorption systems, which are not in common with those studied by the Keck telescope, and failed to reproduce Murphy et al.'s result. At first, they claimed a very stringent limit of  $\Delta\alpha/\alpha = -0.6 \pm 0.6$  ppm, but Murphy et al. (2008a) demonstrated convincingly that the error estimate of Chand et al. (2004) is underestimated. When these errors are properly accounted for, the new weighted mean becomes  $\Delta\alpha/\alpha = -6.4 \pm 3.6$  ppm. The new value has a scatter that is larger than the quoted errors implying that there are systematic errors that are comparable or even larger than the statistical ones. However, Srikanand et al. (2008) showed that excluding two systems that deviate from the mean at the  $3\sigma$  level when reanalyzing VLT/UVES systems leads to  $\Delta\alpha/\alpha = 0.1 \pm 1.5$  ppm. We note that the only claimed non-zero measurement of  $\Delta\alpha/\alpha$  corresponds to an uncertainty in the wavelength scale calibration smaller  $100 \text{ m s}^{-1}$ . This precise calibration of the Keck/HIRES spectra is difficult to achieve as shown by Griest et al. (2010). Using iodine exposures to calibrate the normal Th-Ar Keck data pipeline output, they found absolute wavelength offsets of  $500 \text{ m s}^{-1}$  to  $1000 \text{ m s}^{-1}$  with drifts of more than  $500 \text{ m s}^{-1}$  over a single night, and drifts of nearly  $2000 \text{ m s}^{-1}$  over several nights. Their conclusion is that these systematic uncertainties make it difficult to use Keck/HIRES QSO spectra to constrain the change in the

fine structure constant at the  $10^{-6}$  level. The most stringent constraint on  $|\Delta\alpha/\alpha| < 2$  ppm was found from the Fe II lines at  $z = 1.15$  towards the bright quasar HE 0515-4414 (Quast et al. 2004; Levshakov et al. 2005; Molaro et al. 2008).

Bounds on  $\mu$  variations are most effectively obtained from observations of the Werner and Lyman series of the molecular hydrogen  $\text{H}_2$  in damped Ly- $\alpha$  systems (DLA). The electron-vibro-rotational transitions have different dependences on the reduced mass and can be used to constrain the variability of  $\mu$  (Thompson 1975; Varshalovich & Levshakov 1993). The measurements of  $\mu$  rely on the same  $\text{H}_2$  systems observed with VLT/UVES and claim a variability of  $\Delta\mu/\mu = 24 \pm 6$  ppm (Reinhold et al. 2006) or no variability with  $-15 \text{ ppm} < \Delta\mu/\mu < 57$  ppm (Levshakov et al. 2002),  $|\Delta\mu/\mu| \leq 49$  ppm (Wendt & Reimers 2008),  $\Delta\mu/\mu = 2.6 \pm 3.0$  ppm (King et al. 2008), and  $\Delta\mu/\mu = -7 \pm 8$  ppm (Thompson et al. 2009). Radio astronomical observations place constraints on  $\mu$ -variations of  $|\Delta\mu/\mu| < 1.8$  ppm at redshift  $z = 0.68$  (Murphy et al. 2008b), and  $|\Delta\mu/\mu| < 0.6$  ppm at  $z = 0.89$  (Henkel et al. 2009).

One should keep in mind, however, that laboratory experiments and spectra of extragalactic objects probe very different time-scales and different regions of the universe, and the connection between them is quite model dependent (Mota & Barrow 2004).

Astronomical measurements of the dimensionless constants are based on the comparison of the line centers in the absorption/emission spectra of astronomical objects and the corresponding laboratory values. To distinguish the line shifts due to the radial motion of the object from those caused by the variability of constants, lines with different sensitivity coefficients,  $Q$ , to the variations in  $\mu$  and/or  $\alpha$  should be employed. Unfortunately, the observable optical lines have very close sensitivity coefficients with differences of  $|\Delta Q|$  that do not exceed 0.05. Combined with the resolving power of spectrographs at modern optical telescopes, this small difference leads to an upper limit on  $\Delta\alpha/\alpha$  and  $\Delta\mu/\mu$  of  $\sim 1$  ppm, the optimal value achievable in observations of extragalactic objects with existing facilities. However, one can probe the values of fundamental constants at a considerably more accurate level if, firstly, nearby objects in the Milky Way are observed and, secondly, spectral lines from other frequency ranges, infrared and radio, are employed. This statement is based on the following considerations.

As mentioned above, the scalar field models suggest a coupling between the scalar fields and baryonic matter. This coupling results in a functional dependence of  $\mu$  and  $\alpha$  on  $\rho$ , the local matter density (Olive & Pospelov 2008). This coupling alone may prevent a positive detection of the variations in  $\mu$  and other dimensionless constants in laboratory studies, since they are performed under the same terrestrial conditions and the effective range of the scalar-field-mediated force is smaller than 1 mm at terrestrial matter densities (Olive & Pospelov 2008). On the other hand, the density in cold molecular clouds is only  $10^3 - 10^5$  particles per  $\text{cm}^3$ , i.e.,  $\sim 10^{19}$  times lower than in terrestrial environments. Because of this extremely large difference between the matter densities non-zero values of  $\Delta\mu/\mu$  and  $\Delta\alpha/\alpha$  are predicted. It is very important to compare the above ratio of  $\sim 10^{19}$  with the differences in  $\rho$  between molecular clouds themselves, to find that they are negligible, i.e.,

at most one or two orders of magnitude for a given tracer. In the context of  $\Delta\mu/\mu$  (or  $\Delta\alpha/\alpha$ ) this means that measurements of all dense molecular clouds are identical irrespective of their location in space and time (redshift). Thus, nearby Galactic molecular clouds can be observed to ensure a strong signal, i.e., that the line profiles can be centered with high accuracy.

Molecular lines originating in these clouds are mainly observed in cm and mm radio bands. An advantage of radio observations is that very narrow spectral lines (of line widths  $\sim 100 \text{ m s}^{-1}$ ) arising in cold molecular cores can be observed with extremely high spectral resolution, FWHM  $\sim 25 \text{ m s}^{-1}$ . In optical observations of extragalactic objects, we have in general broader sources,  $b \gtrsim 1 \text{ km s}^{-1}$ , and use lower resolution spectrographs, FWHM  $\gtrsim 4 \text{ km s}^{-1}$  (Levshakov et al. 2007). Taking into account that the uncertainty in the line position is roughly 1/10th of the pixel size, this infers a gain of about two orders of magnitude in the accuracy of the measurements of  $\Delta\alpha/\alpha$  and/or  $\Delta\mu/\mu$  if radio spectra of the local interstellar objects are used.

Complementary to this, differences in the sensitivity coefficients for lines from the microwave, far IR, and radio ranges are much larger than those from optical and UV ranges. For example, the difference between the sensitivity coefficient of the  $(J, K) = (1, 1)$  inversion transition of ammonia ( $\text{NH}_3$ ) and that of any rotational transition in another molecule is  $\Delta Q = 4.46 - 1 = 3.46$  (Flambaum & Kozlov 2007). When compared with UV transitions, this infers a gain of about 70 times in the sensitivity of the line positions to the change in  $\mu$ .

Our preliminary study of cold molecular clouds (Levshakov et al. 2008a, hereafter LMK) was based on published results of high quality spectral radio observations obtained with the 100-m Green Bank telescope (Rosolowsky et al. 2008; Rathborne et al. 2008) and the 45-m Nobeyama radio telescope (Sakai et al. 2008). Comparison of the relative radial velocities of the  $\text{NH}_3$   $(J, K) = (1, 1)$  inversion transition and CCS  $J_N = 2_1 - 1_0$  rotational transition measured a systematic shift of  $\Delta V \equiv V_{\text{lsr}}(\text{CCS}) - V_{\text{lsr}}(\text{NH}_3) \sim 60 \text{ m s}^{-1}$ , which when interpreted in terms of the electron-to-proton mass ratio variation infers that  $\Delta\mu/\mu \sim 6 \times 10^{-8}$ . We also noted that a similar offset between  $\text{N}_2\text{H}^+$  and  $\text{NH}_3$  measured by Pagani et al. (2009) in the cold dark cloud L183 could have a similar physical origin (Molaro et al. 2009).

In this paper, we present results of our own spectral observations of cold and compact molecular cores in the Taurus giant molecular complex obtained with the Medicina 32-m telescope, the Effelsberg 100-m telescope, and the Nobeyama 45-m telescope.

## 2. The ammonia method

Narrow molecular lines observed in cold dark clouds provide a sensitive spectroscopic tool to study relative shifts of the order of a few  $10 \text{ m s}^{-1}$  between radial velocities of different molecular transitions. Among numerous molecules detected in the interstellar medium, ammonia ( $\text{NH}_3$ ) is of particular interest because of the high sensitivity of the inversion frequency to a change in  $\mu$ . The inversion vibrational mode of  $\text{NH}_3$  is described by a double-well potential, the first two vibrational levels lying below the barrier. The quantum mechanical tunneling splits these two levels into inversion

doublets providing a transition frequency that falls in the microwave range (Ho & Townes 1983).

For the ammonia isotopologue  $^{15}\text{ND}_3$ , van Veldhoven et al. (2004) first showed that the inversion frequency of the  $(J, K) = (1, 1)$  level varies as<sup>1</sup>

$$\left(\frac{\Delta\nu}{\nu}\right)_{\text{inv}} = 5.6 \frac{\Delta\mu}{\mu}, \quad (1)$$

i.e., the inversion transition is an order of magnitude more sensitive to  $\mu$ -variation than molecular vibrational transitions, which scale as  $E_{\text{vib}} \sim \mu^{1/2}$ .

The sensitivity coefficient of the inversion transition  $(J, K) = (1, 1)$  in  $\text{NH}_3$  ( $\nu = 23.7 \text{ GHz}$ ) was calculated by Flambaum & Kozlov (2007) from the numerical integration of the Schrödinger equation for different values of  $\mu$ , and from the analytical Wentzel-Kramers-Brillouin (WKB) approximation of the inversion frequency. Both methods provide similar results giving

$$\left(\frac{\Delta\nu}{\nu}\right)_{\text{inv}} \equiv \frac{\tilde{\nu} - \nu}{\nu} = 4.46 \frac{\Delta\mu}{\mu}. \quad (2)$$

Here  $\nu$  and  $\tilde{\nu}$  are the frequencies corresponding to the laboratory value of  $\mu$  and to an altered  $\mu$  in a low-density environment, respectively.

The rotational frequency scales as  $E_{\text{rot}} \sim \mu$  and, thus,

$$\left(\frac{\Delta\nu}{\nu}\right)_{\text{rot}} \equiv \frac{\tilde{\nu} - \nu}{\nu} = \frac{\Delta\mu}{\mu}. \quad (3)$$

By comparing the observed inversion frequency of  $\text{NH}_3$  (1,1) with a suitable rotational frequency of another molecule produced *co-spatially* with ammonia, a limit on the spatial variation of  $\mu$  can be determined.

In radio astronomical observations, any frequency shift  $\Delta\nu$  is related to the radial velocity shift  $\Delta V_r$  ( $V_r$  is the line-of-sight projection of the velocity vector)

$$\frac{\Delta V_r}{c} \equiv \frac{V_r - V_0}{c} = \frac{\nu_{\text{lab}} - \nu_{\text{obs}}}{\nu_{\text{lab}}}, \quad (4)$$

where  $V_0$  is the reference radial velocity, and  $\nu_{\text{lab}}$ ,  $\nu_{\text{obs}}$  are the laboratory and observed frequencies, respectively. Therefore, by comparing the apparent radial velocity  $V_{\text{inv}}$  for the  $\text{NH}_3$  inversion transition with the apparent radial velocity  $V_{\text{rot}}$  for rotational lines originating in the same molecular cloud and moving with a radial velocity  $V_0$  with respect to the local standard of rest, we can find from Eqs. (2 - 4)

$$\frac{\Delta\mu}{\mu} = 0.289 \frac{V_{\text{rot}} - V_{\text{inv}}}{c} \equiv 0.289 \frac{\Delta V}{c}. \quad (5)$$

From Eq.(5), we can estimate the limiting accuracy of  $\Delta\mu/\mu$  available from modern radio astronomical observations. At high spectral resolution in the microwave range (FWHM  $\sim 30 \text{ m s}^{-1}$ ), the errors in the molecular line position measurements are mainly restricted by the uncertainties in laboratory frequencies,  $\varepsilon_\nu \sim 0.1 - 1 \text{ kHz}$ , which correspond to the  $V_{\text{lsr}}$  uncertainties of  $\varepsilon_v \sim 1 - 10 \text{ m s}^{-1}$ . Taking into account that  $\Delta\mu/\mu \sim 0.3\Delta V/c$ , the expected accuracy of  $\Delta\mu/\mu$  in a single measurement is about  $10^{-8}$ .

<sup>1</sup> The sign of the sensitivity coefficient  $Q = 5.6$  was misprinted in van Veldhoven et al. (2004), as noted by Flambaum & Kozlov (2007).

This level of accuracy can be achieved, however, only under ideal conditions since it assumes that molecules are identically distributed within the cloud and are observed simultaneously with the same receiver, beam size, system temperature, and velocity resolution. Violation of any of these conditions leads to random shifts of the line centers, which are referred to as the *Doppler noise*. The input of the Doppler noise to a putative  $\Delta\mu/\mu$  signal can be reduced to some extent if the velocity shifts due to the inhomogeneous distribution of molecules and to instrumental imperfections are minimized. For our purposes, we express the velocity offset  $\Delta V$  in Eq.(5) as the sum of two components

$$\Delta V = \Delta V_\mu + \Delta V_n, \quad (6)$$

where  $\Delta V_\mu$  is the shift due to  $\mu$ -variation and  $\Delta V_n$  is the Doppler noise. We assume that the noise component has zero mean  $\langle \Delta V_n \rangle = 0 \text{ km s}^{-1}$  and a finite variance. The signal  $\Delta V_\mu$  can then be estimated statistically by averaging over a data sample

$$\langle \Delta V \rangle = \langle \Delta V_\mu \rangle, \quad \text{Var}(\Delta V) = \text{Var}(\Delta V_\mu) + \text{Var}(\Delta V_n). \quad (7)$$

From this equation it is seen that the measurability of the signal ( $\Delta V_\mu$ ) depends critically on the value of the Doppler noise. The Doppler noise  $\text{Var}(\Delta V_n)$  can be reduced by an appropriate choice of molecular lines and by special criteria applied to the selection of targets.

### 2.1. Molecules appropriate for $\Delta\mu/\mu$ measurements

The observed molecular transitions should as far as possible share the same volume elements to have similar Doppler velocity shifts. The ammonia inversion transitions are usually detected in dense molecular cores ( $n \gtrsim 10^4 \text{ cm}^{-3}$ ), which are represented in the Milky Way disk by a large variety of types and physical properties (Di Francesco et al. 2007). Mapping of the dense molecular cores in different molecular lines shows that there is a good correlation between the ammonia  $\text{NH}_3$ ,  $\text{N}_2\text{H}^+$ , and  $\text{HC}_3\text{N}$  distributions (e.g., Fuller & Myers 1993; Hotzel et al. 2004; Tafalla et al. 2004; Pagani et al. 2009). However, in some clouds  $\text{NH}_3$  is not traced by  $\text{HC}_3\text{N}$ . The most striking case is the dark cloud TMC-1, where peaks of line emission are offset by 7 arcmin (Olano et al. 1988).

In general, N-bearing molecules such as  $\text{NH}_3$  and  $\text{N}_2\text{H}^+$  trace the inner cores, where the density approaches  $10^5 \text{ cm}^{-3}$ . At the same time, the carbon-chain molecules disappear from the gas-phase because of freeze-out onto dust grains (Tafalla et al. 2004).  $\text{HC}_3\text{N}$ , as well as other C-bearing molecules, are usually distributed in the outer parts of the cores. The mutual distribution of  $\text{NH}_3$  and  $\text{HC}_3\text{N}$  is affected by chemical differentiation in the process of the dynamical evolution of the core.  $\text{HC}_3\text{N}$  is abundant in the early evolutionary stage of the star-forming regions (Lee et al. 1996), when the fractional abundance of  $\text{HC}_3\text{N}$  remains almost constant and the spatial distributions of the N- and C-bearing molecules match each other quite well (Suzuki et al. 1992). As the gas density increases and at dust temperatures  $T_d < 20 \text{ K}$ , these distributions diverge because of adsorption of the heavy molecules (e.g.,  $\text{HC}_3\text{N}$ ) from the gas phase onto grain mantles (Flower et al. 2006). In the later stages of the protostellar collapse, carbon chain molecules are destroyed by high velocity outflows and radiation from protostars, whereas the same processes favor the desorption of ammonia from dust grains (Suzuki et al. 1992).

The chemical differentiation and velocity gradients within the molecular core are the main sources of the unavoidable Doppler noise in Eq.(6). Additional scatter in the  $\Delta V_n$  values is caused by the different optical depths of the hyperfine structure transitions. However, all of these effects lead to the radial velocity shifts detected between  $\text{NH}_3$  and other molecules ( $\text{HC}_3\text{N}$ ,  $\text{N}_2\text{H}^+$ ), which may be random from core to core. Thus, being averaged over a large sample of targets, the Doppler noise component  $\Delta V_n$  in Eq. (6) should be canceled out.

### 3. Observations

For relative velocity measurements, the molecular lines of  $\text{NH}_3$ ,  $\text{HC}_3\text{N}$ , and  $\text{N}_2\text{H}^+$  were chosen. From the published data, we selected 41 molecular cores with compact morphology, i.e., the cores whose geometrical structure can be represented by a central region of nearly constant density and a surrounding envelope with a density that decreases as a power law. For the dark clouds in the Taurus molecular complex, a typical size of the central core is  $r_0 \sim 20'' - 60''$  (e.g., Daniel et al. 2007). The selection was based on narrow and sufficiently strong molecular lines that correspond to individual hyperfine transitions:  $\text{NH}_3$  ( $J, K$ ) = (1, 1),  $\text{HC}_3\text{N}$   $J = 2 - 1$ , and  $\text{N}_2\text{H}^+$   $J = 1 - 0$ . This suggests that the selected cores have low kinetic temperatures ( $T_{\text{kin}} \sim 10 \text{ K}$ ) and are located at distances below 250 pc. The kinetic temperature is known to be surprisingly uniform in dark clouds (e.g., Dickman 1975; Walmsley & Ungerechts 1983). The list of sources is given in Table 1. Observations were performed with radio telescopes in Medicina, Effelsberg, and Nobeyama between November 2008 and April 2009.

*Medicina.* Observations at the Medicina 32-m telescope<sup>2</sup> were carried out on November 24-28, 2008. Both available digital spectrometers ARCOS (ARcetri COrrelation Spectrometer) and MSpec0 (high resolution digital spectrometer) were used with channel separations of 4.88 kHz and 2 kHz, respectively. For ARCOS, this corresponds to  $62 \text{ m s}^{-1}$  at the position of the ammonia inversion transition (23 GHz) and  $80 \text{ m s}^{-1}$  at the rotational  $\text{HC}_3\text{N}$  (2-1) line (18 GHz). For MSpec0, it is  $25 \text{ m s}^{-1}$  and  $32 \text{ m s}^{-1}$  at the corresponding frequencies. Only a few brightest objects (marked by a symbol  $m$  in Table 1) were observed. The Medicina 32-m telescope angular resolution is  $\sim 1.6'$  at 23 GHz and  $\sim 2.1'$  at 18 GHz. The pointing accuracy was superior to  $25''$ . Spectra were taken in a position switching mode with a typical integration time of 5 min for both ON- and OFF-source scans. The OFF position was taken to be approximately five beam widths to the west of the source position. Typically, 10-20 ON/OFF pairs were taken, depending on the frequency and source flux. Unfortunately, because of poor weather conditions not all observations studied both  $\text{NH}_3$  and  $\text{HC}_3\text{N}$  transitions. Standard data reduction was performed using the CLASS reduction package<sup>3</sup>.

*Effelsberg.* The ( $J, K$ ) = (1,1) inversion line of ammonia ( $\text{NH}_3$ ) and the  $J=2-1$  rotation line of cyanoacetylene ( $\text{HC}_3\text{N}$ ) were also observed with the 100-m telescope at

<sup>2</sup> The 32-m VLBI antenna at Medicina is operated by the INAF-Istituto di Radioastronomia in Bologna.

<sup>3</sup> <http://www.iram.fr/IRAMFR/GILDAS/>

Effelsberg<sup>4</sup> on February 20–22, 2009. The corresponding targets are marked by symbol  $e$  in Table 1. The lines were measured with a K-band HEMT (high electron mobility transistor) dual channel receiver, yielding spectra with angular resolutions of 40'' (NH<sub>3</sub>) and 50'' (HC<sub>3</sub>N) in two orthogonally oriented linear polarizations. Averaging the emission from both channels, typical system temperatures are 100–150 K for NH<sub>3</sub> and 80–100 K for HC<sub>3</sub>N on a main beam brightness temperature scale.

The measurements were carried out in frequency switching mode using a frequency throw of  $\sim 5$  MHz. The backend was an FFTS (fast fourier transform spectrometer), operated with its minimum bandwidth of 20 MHz, providing simultaneously 16 384 channels for each polarization. The resulting channel widths are 15.4 and 20.1 m s<sup>-1</sup> for NH<sub>3</sub> and HC<sub>3</sub>N, respectively. We note, however, that the true velocity resolution is about twice as large.

Observations started by measuring the continuum emission of calibration sources (NGC 7027, W3(OH), 3C 286) and continued by performing pointing measurements toward a source close to the spectroscopic target. Spectral line measurements were interspersed with pointing measurements at least once per hour. The calibration is estimated to be accurate to  $\pm 15\%$  and the pointing accuracy to be superior to 10 arcsec. The CLASS reduction package was used for standard data reduction.

*Nobeyama.* The NH<sub>3</sub> ( $J, K$ ) = (1, 1) line at 23 GHz and the N<sub>2</sub>H<sup>+</sup>  $J=1-0$  line at 93 GHz were observed with the Nobeyama Radio Observatory (NRO) 45-m telescope<sup>5</sup> on April 8–10, 2009. We used a low-noise HEMT receiver, H22, for the NH<sub>3</sub> observations and the two sideband-separating SIS (Superconductor-Insulator-Superconductor) receiver, T100 (Nakajima et al. 2008), for the N<sub>2</sub>H<sup>+</sup> observations. Both of them are dual polarization receivers. We observed two polarizations simultaneously. The 45-m radio telescope angular resolution is about 73 and 17 arcsec at 23 and 93 GHz, respectively, and the main beam efficiency is 0.84 at 23 GHz, and 0.53 at 93 GHz. Autocorrelators were employed as a backend with bandwidth and channel separation of 4 MHz and 4.375 kHz, respectively. This corresponds to channel widths of 57 m s<sup>-1</sup> at 23 GHz, and 14 m s<sup>-1</sup> at 93 GHz.

The telescope pointing was checked by observing nearby SiO maser sources every 1–2 hr. The pointing accuracy was  $\leq 5''$ . The line intensities were calibrated using the chopper wheel method, and the observations were carried out in position switching mode. The data reduction was performed partly with the AIPS-based software package NewStar developed at NRO.

## 4. Data analysis

### 4.1. $V_{lsr}$ calculation

The radial velocities,  $V_{lsr}$ , are determined from the spectral line analysis. Each individual exposure was first visually analyzed and corrupted data were excluded. Individual exposures were then coadded to increase the signal-to-noise

<sup>4</sup> The 100-m telescope at Effelsberg/Germany is operated by the Max-Planck-Institut für Radioastronomie on behalf of the Max-Planck-Gesellschaft (MPG).

<sup>5</sup> The 45-m radio telescope is operated by Nobeyama Radio Observatory, a branch of the National Astronomical Observatory of Japan.

(S/N) ratio. Before coadding, a baseline was removed from each spectrum. To define the baseline, spectral intervals without emission lines and/or noise spikes were selected and the mean signal  $T_i$  along with its rms uncertainty  $\sigma_i$  were calculated for each interval. A set of pairs  $\{T_i, \sigma_i\}$  was used to find a baseline (regression line) by minimizing  $\chi^2$ . This baseline was typically linear but was in some cases quadratic or cubic. Since individual rms uncertainties  $\sigma_i$  were of the same order of magnitude, their mean value  $\sigma$  was assigned to the whole spectrum. The resulting spectra were coadded with weights that are inversionally proportional to their variances,  $\sigma^2$ .

The line parameters such as the total optical depth in the transition,  $\tau$ , the radial velocity,  $V_{lsr}$ , the line broadening Doppler parameter,  $b$ , and the amplitude,  $A$ , were estimated by fitting a one-component Gaussian model to the observed spectra. The model was defined by

$$T(v) = A \cdot \left[ 1 - e^{-t(v)} \right], \quad (8)$$

where

$$t(v) = \tau \cdot \sum_{i=1}^k a_i \exp \left[ -\frac{(v - v_i - V_{lsr})^2}{b^2} \right], \quad (9)$$

where  $a_i, v_i$  is, respectively, the relative intensity of the  $i$ th hyperfine component and its velocity separation from the reference frequency. The sum in Eq. (9) runs over the  $k$  hyperfine structure (hfs) components of the transition. The physical parameters  $a_i$ , and  $v_i$  for the NH<sub>3</sub> (1,1), HC<sub>3</sub>N (2-1), and N<sub>2</sub>H<sup>+</sup> (1-0) transitions are listed in Tables 2, 3, and 4, respectively.

The fitting parameters  $\{A, \tau, b, V_{lsr}\}$  were determined by means of a  $\chi^2$ -minimization procedure. For optically thin transitions, Eq.(8) transforms into

$$T(v) = A \cdot t(v), \quad (10)$$

which prevents the independent estimation of  $A$  and  $\tau$ . In this case, the model parameters were  $\{A \cdot \tau, b, V_{lsr}\}$ .

Since we are mostly interested in the model parameters  $V_{lsr}$  and  $b$ , their values are listed in Tables 5 and 6. The  $1\sigma$  errors of  $V_{lsr}$  and  $b$  were estimated from the diagonal elements of the covariance matrix calculated for the minimum of  $\chi^2$ . The error in  $V_{lsr}$  was also estimated independently by the  $\Delta\chi^2$  method (e.g., Press et al. 1992) to control both results. When two estimates differed, the larger error was adopted.

### 4.2. Uncertainties in the rest-frequencies

Molecular lines observed in cold dark clouds of  $T_{\text{kin}} \sim 10$ K can be extremely narrow with a thermal broadening of  $v_{\text{th}} \lesssim 100$  m s<sup>-1</sup> for NH<sub>3</sub> or even lower for heavier molecules. They provide a sensitive spectroscopic measurement of shallow velocity gradients in molecular clouds (Lapinov 2006). At high spectral resolution ( $FWHM \sim 30$  m s<sup>-1</sup>), the uncertainty in the line position measurement from radio astronomical observations can be as small as 1 m s<sup>-1</sup> which is comparable to the precision available for laboratory rest-frame frequencies of the NH<sub>3</sub> ( $J, K$ ) = (1, 1) transition (Kukulich 1967; Hougen 1972). The physical parameters of the observed hfs components of NH<sub>3</sub> are listed in Table 2. Column 1 indicates the group numbers

shown in the upper panel of Fig. 2. The errors in the line positions given in parentheses in Col. 7 are smaller than  $1 \text{ m s}^{-1}$  with a mean of  $\varepsilon_v = 0.58 \text{ m s}^{-1}$ . However, laboratory uncertainties for other molecules used in the present observations are significantly larger.

The analysis of all available laboratory data about  $\text{HC}_3\text{N}$  carried out by Müller et al. (2005) and independently by Lapinov (2008, private comm.) shows good agreement, the latter results being of slightly higher precision ( $\varepsilon_v \simeq 2.8 \text{ m s}^{-1}$ ). The physical parameters of the hfs components of the  $J = 2 - 1$  transition are presented in Table 3. The line identification numbers from Col. 1 are depicted in the middle panel of Fig. 2.

The rest-frame frequencies for the third molecule  $\text{N}_2\text{H}^+$  (Table 4) were taken from the Cologne Database for Molecular Spectroscopy (CDMS) described in Müller et al. (2005). The group numbers from Table 4, Col. 1 are also shown in Fig. 2, lower panel. The CDMS data have a factor of two smaller errors than the hyperfine frequencies estimated from observations of the molecular core L1512 in both  $\text{N}_2\text{H}^+$  (93 GHz) and  $\text{C}_3\text{H}_2$  (85 GHz). It is again assumed that these molecules are co-spatially distributed (Caselli et al. 1995). The error in  $\varepsilon_v \simeq 13.5 \text{ m s}^{-1}$  ( $\simeq 4 \text{ kHz}$ ) reported in Table 4 corresponds to the CDMS data. The mean offset between the data from Caselli et al. and the CDMS is  $\Delta V = V_{\text{Caselli}} - V_{\text{CDMS}} = 12 \text{ m s}^{-1}$ .

We do not correct the  $\text{N}_2\text{H}^+$  frequencies for a  $40 \text{ m s}^{-1}$  offset as by Pagani et al. (2009), who used the rest-frame frequencies of Caselli et al.. The offset of  $40 \text{ m s}^{-1}$ , or  $28 \text{ m s}^{-1}$  when adopting the CDMS rest frequencies (Molaro et al. 2009), was determined by comparing the inversion  $\text{NH}_3$  (1,1) and rotational  $\text{N}_2\text{H}^+$  (1-0) transitions observed in the target L183; this correction is justifiable only when  $\Delta\mu/\mu \equiv 0$ . Reliable calibrations of the hyperfine transition frequencies of  $\text{N}_2\text{H}^+$  can be performed only by a high precision laboratory measurement.

We note in passing that the estimate of the mean radial velocity based on the simultaneous fitting of  $n$  hyperfine transitions should be more precise than that based on a single line. However, the improvement is not as high as  $1/\sqrt{n}$  because the relative positions of the individual hfs transitions are correlated. If we consider  $n$  velocity differences  $\{v_1 - v_0, v_2 - v_0, \dots, v_n - v_0\}$ , where  $v_0$  is the reference velocity, then it is easy to show that the correlation coefficient  $\kappa_{i,j}$  between two of them ( $i \neq j$ ) is given by

$$\kappa_{i,j} = \frac{1}{\sqrt{(1 + s_i^2)(1 + s_j^2)}}, \quad (11)$$

where  $s_i = \sigma_{v_i}/\sigma_{v_0}$  and  $s_j = \sigma_{v_j}/\sigma_{v_0}$ . Taking into account that the laboratory errors in the hyperfine line positions,  $\sigma_{v_i}$ , are almost equal, we have  $\kappa_{i,j} = \kappa \approx 1/2$ .

The covariance matrix  $\text{Cov}(v_i - v_0, v_j - v_0)$  contains  $n$  diagonal terms  $\sigma^2$  and  $n(n-1)$  non-diagonal terms  $\kappa\sigma^2$ , where  $\sigma^2$  represents the variance in a single measurement. The error in the mean radial velocity caused by the laboratory uncertainties (referred to as  $\varepsilon_{\text{sys}}$  hereafter) can be calculated as described by, e.g., Stuart & Ord (1994)

$$\varepsilon_{\text{sys}} = \left[ \sum_{i=1}^n \sum_{j=1}^n \omega_i \omega_j \text{Cov}(v_i - v_0, v_j - v_0) \right]^{1/2}. \quad (12)$$

In cases of equal accuracy, the weight  $\omega_i = 1/n$  for each  $i$ . Then  $\varepsilon_{\text{sys}}$  is approximately equal to

$$\varepsilon_{\text{sys}} = \frac{\sigma}{n} \sqrt{n + n(n-1)\kappa} \approx \sigma \sqrt{\kappa}. \quad (13)$$

Thus, the gain factor,  $\sqrt{\kappa}$ , is only about 0.7 for the molecules in question.

## 5. Results

We first consider the entire sample of sources listed in Table 1. By applying the same computational procedure to all available spectra from the three radio telescopes, we find that not all of the molecular profiles can be described adequately with a single-component Gaussian model. In total, we measured  $n = 55$  molecular pairs. The corresponding velocity offsets  $\Delta V$  are shown in Fig. 10 by three types of symbols: filled squares and circles ( $\text{NH}_3/\text{HC}_3\text{N}$  pairs), and open circles ( $\text{NH}_3/\text{N}_2\text{H}^+$  pairs) are, respectively, data points from the 32-m, 100-m, and 45-m telescopes. Some molecular cores (L183, L1495, TMC-1C) were partially mapped. The offset coordinates in arcsec with respect to the source positions from Table 1 are shown in parentheses. Two objects (L183 and TMC-1C) were observed at the 32-m telescope with different spectrometers ARCOS and MSpec0, as indicated in the figure. Five sources, TMC-1/ $\text{HC}_3\text{N}$  (Medicina), TMC-2, L1521F, and L1544 (Effelsberg), and TMC-2 (Nobeyama) from Table 1 exhibit asymmetric profiles that are not consistent with a simple Gaussian model (we do not show them in Fig. 10). A considerable fraction of the molecular pairs from the total sample exhibit non-thermal motion, i.e., the Doppler broadening parameter  $b(\text{NH}_3) \leq b(\text{HC}_3\text{N}, \text{N}_2\text{H}^+)$ .

Several sources were observed at different radio telescopes. Since these data points have different systematic errors, we treat them as ‘independent’ measurements in the following statistical estimates.

The weighted mean (weights inversionally proportional to the variances) of the ensemble of  $n = 55$   $\Delta V$  values is  $\langle \Delta V \rangle_{\text{w}} = 27.4 \pm 4.4 \text{ m s}^{-1}$ , the scale (standard deviation) is  $32.6 \text{ m s}^{-1}$ , and the median is  $17 \text{ m s}^{-1}$ . We also used a robust redescending  $M$ -estimate for the mean and the normalized median absolute deviation (1.483-MAD) for the scale. These statistics work well for inhomogeneous data sets with outliers and deviations from normality (corresponding formulae are given in Appendix). The  $M$ -estimate infers that  $\langle \Delta V \rangle_{\text{M}} = 14.1 \pm 4.0 \text{ m s}^{-1}$  (scale  $29.6 \text{ m s}^{-1}$ ). A poor concordance between three mean estimates ( $\langle \Delta V \rangle_{\text{w}}$ ,  $\langle \Delta V \rangle_{\text{M}}$ , and the median) is caused by large systematic shifts and, as a result, by ‘heavy tails’ of the probability distribution function. The scatter in the points reflects effects related to the gas kinematics and the chemical segregation of one molecule with respect to the other.

An additional decrease in the noise component  $\text{Var}(\Delta V_n)$  in Eq. (7) is possible if we select from the sample of the observed targets the systems with ‘simple’ geometry and internal kinematics. The ideal target would be a homogeneous spherical cloud where different molecules are co-spatially distributed (no chemical segregation) and where turbulence is suppressed (thermally dominated motion). In this case, any deviations from the expected zero mean value of the radial velocity difference between rotational and inversion molecular transitions in Eq. (5) could be ascribed to the non-zero  $\Delta\mu$  value.

In practice, molecular cores are not ideal spheres and when observed at higher angular resolutions they frequently exhibit complex substructures. The line profiles may be asymmetric because of non-thermal bulk motions. Taking this into account, the following criteria were formulated:

1. The line profiles are symmetric described well by a single-component Gaussian model (i.e., the minimum value of  $\chi_\nu^2 \sim 1$ ). This selection increases the accuracy of the line center measurement. Multiple line components may shift the line barycenter and affect the velocity difference between molecular transitions because, e.g., the ratio  $\text{NH}_3/\text{HC}_3\text{N}$  can vary from one component to another.
2. The line widths do not greatly exceed the Doppler width because of the thermal motion of material, i.e., the non-thermal component (infall, outflow, tidal flow, turbulence) does not dominate the line broadening. This ensures that selected molecular lines correspond to the same kinetic temperature and arise cospatially. For the molecules in question we require that the ratio of the Doppler  $b$ -parameters,  $\beta = b(\text{NH}_3)/b(\text{HC}_3\text{N})$  or  $\beta = b(\text{NH}_3)/b(\text{N}_2\text{H}^+)$ , be  $\beta \geq 1$ .
3. The spectral lines are sufficiently narrow ( $b \sim 0.1 - 0.2 \text{ km s}^{-1}$ ) for hyperfine structure components to be resolved. This allows us to validate the measured radial velocity by means of different hfs lines of the same molecular transition.
4. The spectral lines are not heavily saturated and their profiles are not affected by optical depth effects. The total optical depth of the  $\text{NH}_3$  hf transitions is  $\tau \leq 10$ .

We now consider molecular lines that fulfill these additional selection criteria. Among the sources listed in Table 1, two and twelve molecular cores can be selected from, respectively, the Medicina and Effelsberg observations (Table 5), and nine clouds from the Nobeyama data set (Table 6). The sample size is now  $n = 23$ , i.e., two times smaller than the total data set.

Table 5 lists the values obtained from the analysis of the  $\text{NH}_3$  (1,1) and  $\text{HC}_3\text{N}$  (2-1) transitions, whereas in Table 6 the  $\text{NH}_3$  (1,1) and  $\text{N}_2\text{H}^+$  (1-0) measurements are presented. Where individual hfs transitions can be analyzed separately, the results of these analyses are also given. The data obtained for  $\text{NH}_3$  are divided formally into 4 groups, which are marked in Fig. 1 and Table 2 by the following numbers: ‘outer’ – 1 and 5, ‘inner’ – 2 and 4, ‘central’ – 3, and ‘total’ combines all hfs lines (Cols. 2-5 of Table 5, respectively). For  $\text{HC}_3\text{N}$ , the measurements are presented in 3 groups, which are marked in Fig. 1 and Table 3 as: ‘low’ – 1, 5, and 6, ‘high’ – 3 and 4, and ‘total’ – 1, 3, 4, 5, and 6 (Cols. 6-8 of Table 5, respectively). Line number 2 ( $F = 1 - 2$ ) is very weak and was never detected in our observations. For  $\text{N}_2\text{H}^+$ , we divided the hfs lines into 3 groups on the basis of their relative theoretical intensities. These groups are indicated in Fig. 1 and Table 4 as: ‘low’ – 1, 2, 5, and 7, ‘high’ – 3, 4, and 6, and ‘total’ combines all hfs lines (Cols. 6-8 of Table 6, respectively).

The analyzed molecular line profiles are shown in Figs. 2-9. The smooth curves are synthetic spectra calculated in the simultaneous fit of all hyperfine components to the observed profiles. Bold horizontal lines mark the spectral ranges included in the  $\chi^2$ -minimization procedure. The quality of individual fittings can be characterized by the normalized  $\chi_\nu^2$  values given in Tables 5 and 6 for each group

of measurements. The residuals ‘observed data – model’ are depicted beneath each spectrum in Figs. 2-9. The signal-to-noise ratio (S/N) per resolution element shown in these figures is calculated at the maximum intensity peak.

The velocity offsets,  $\Delta V$ , and their statistical errors are listed in Col. 9 of Tables 5 and 6. When calculating  $\Delta V$ , we used the mean  $V_{lsr}$  radial velocities based on the simultaneous fitting of all hyperfine transitions. The  $\Delta V$  values estimated in 23 measurements are marked in Fig. 11 by the circles with  $1\sigma$  error bars. The filled circles indicate sources with thermally dominated motions. We also show the ratios of the Doppler  $b$ -parameters:  $\beta = b(\text{NH}_3)/b(\text{HC}_3\text{N})$  or  $\beta = b(\text{NH}_3)/b(\text{N}_2\text{H}^+)$ , in parentheses provide their  $1\sigma$  errors. For the 32-m and 100-m telescopes,  $\Delta V = V_{lsr}(\text{HC}_3\text{N}) - V_{lsr}(\text{NH}_3)$ , whereas for the 45-m telescope  $\Delta V = V_{lsr}(\text{N}_2\text{H}^+) - V_{lsr}(\text{NH}_3)$ .

Among the selected clouds, we discover that only one (L260- $\text{NH}_3$ ) violates the selection rule No. 4. The total optical depth in this case is  $\tau = 15.6$ . We used this cloud since the spectrum of  $\text{NH}_3$  was of high S/N and other selection criteria were fulfilled. We note, however, that this cloud has the minimum  $\Delta V$  value consistent with a zero offset (see Table 5 and Fig. 11).

Both data sets exhibit an excess of positive velocity offsets. The most accurate results are obtained for the L1498 and L1512 molecular cores observed with the 100-m Effelsberg telescope,  $\Delta V = 21.0 \pm 1.5 \text{ m s}^{-1}$ . In this case, the systematic error due to the rest frequency uncertainties does not exceed  $3 \text{ m s}^{-1}$ . The maximum spread between the individual hfs  $V_{lsr}$  velocities for  $\text{NH}_3$  is  $5.5 \text{ m s}^{-1}$  (L1498) and  $4.5 \text{ m s}^{-1}$  (L1512), but it is only  $1.0 \text{ m s}^{-1}$  for the  $\text{HC}_3\text{N}$  hyperfine transitions in both sources. The molecular lines are narrow with  $b(\text{NH}_3) = 118 \pm 1 \text{ m s}^{-1}$ ,  $b(\text{HC}_3\text{N}) = 91 \pm 5 \text{ m s}^{-1}$  (L1498), and  $b(\text{NH}_3) = 113 \pm 1 \text{ m s}^{-1}$ ,  $b(\text{HC}_3\text{N}) = 79 \pm 4 \text{ m s}^{-1}$  (L1512), which is in line with the assumption that in these two clouds both molecules trace the same volume elements.

The sources with thermally dominated motions ( $n = 7$ ) marked by the filled circles in Fig. 11 give the weighted mean of  $\langle \Delta V \rangle_w = 21.1 \pm 1.3 \text{ m s}^{-1}$ , the scale  $3.4 \text{ m s}^{-1}$ , and the median  $22 \text{ m s}^{-1}$ . The corresponding  $M$ -estimate is  $\langle \Delta V \rangle_M = 21.2 \pm 1.8 \text{ m s}^{-1}$  (scale  $4.8 \text{ m s}^{-1}$ ).

For the ensemble of  $n = 23$   $\Delta V$  values, we found the weighted mean of  $\langle \Delta V \rangle_w = 20.7 \pm 3.0 \text{ m s}^{-1}$ , the scale  $14.4 \text{ m s}^{-1}$ , and the median  $22 \text{ m s}^{-1}$ . The robust  $M$ -estimate is  $\langle \Delta V \rangle_M = 21.5 \pm 2.8 \text{ m s}^{-1}$  (scale  $13.4 \text{ m s}^{-1}$ ). Thus, in the reduced sample, we have good agreement between all three estimates of the mean. The scatter in the points (the Doppler noise) is lower by a factor of two than that of the  $n = 55$  data set.

The individual data from the 100-m and 45-m telescopes provide the following estimates. *Effelsberg*:  $\langle \Delta V \rangle_w = 23.0 \pm 3.1 \text{ m s}^{-1}$  ( $n = 12$ , scale  $10.7 \text{ m s}^{-1}$ , median  $22 \text{ m s}^{-1}$ ),  $\langle \Delta V \rangle_M = 23.2 \pm 3.8 \text{ m s}^{-1}$  (scale  $13.3 \text{ m s}^{-1}$ ). *Nobeyama*:  $\langle \Delta V \rangle_w = 14.0 \pm 7.2 \text{ m s}^{-1}$  ( $n = 9$ , scale  $21.6 \text{ m s}^{-1}$ , median  $22 \text{ m s}^{-1}$ ),  $\langle \Delta V \rangle_M = 22.9 \pm 4.2 \text{ m s}^{-1}$  (scale  $12.7 \text{ m s}^{-1}$ ).

Although the robust  $M$ -estimates of the mean for both the Effelsberg and Nobeyama observations are consistent, the latter has a larger systematic error due to its lower accuracy at the rest frequencies of the  $\text{N}_2\text{H}^+$  (1-0) transition. Taking into account that the rest frequencies of the  $\text{HC}_3\text{N}$  (2-1) are known with a sufficiently high accuracy (the uncertainties in the laboratory and observational frequencies are comparable), we take the Effelsberg robust mean as

a final value for the velocity offset between the rotational and inversion transitions. Being interpreted in terms of the electron-to-proton mass ratio variation, this provides the value  $\Delta\mu/\mu = 22 \pm 4_{\text{stat}} \pm 3_{\text{sys}}$  ppb (1 ppb =  $10^{-9}$ ).

### 5.1. Data reproducibility

Taking into account numerous perturbation effects discussed above and variations in specific parameters such as spectral resolution and signal-to-noise ratio, we question the consistency of the measured  $\Delta V$  values obtained for independent telescope systems. This consistency was first tested at the 32-m Medicina telescope, where we observed two cores, L183 and TMC-1C, in lines of  $\text{NH}_3$  (1,1) and  $\text{HC}_3\text{N}$  (2-1) with the ARCOS and MSpec0 digital spectrometers. For L183, we found  $\Delta V = 6 \pm 7 \text{ m s}^{-1}$  (MSpec0) and  $-4 \pm 15 \text{ m s}^{-1}$  (ARCOS), whereas for TMC-1C, the corresponding quantities were measured to be  $67.5 \pm 5.8 \text{ m s}^{-1}$  and  $68.5 \pm 3.2 \text{ m s}^{-1}$ . Both results are in good agreement to within the  $1\sigma$  uncertainty interval.

We also tested the reliability of the velocity offsets by obtaining observations of the same cores at different telescopes. For instance, a quiescent low-mass molecular core L1512 in the Taurus Cloud was observed in the  $\text{NH}_3$  (1,1) and  $\text{HC}_3\text{N}$  (2-1) lines at the 32-m and 100-m telescopes. The corresponding velocity offsets are  $\Delta V = 17.5 \pm 4.1 \text{ m s}^{-1}$  and  $20.5 \pm 1.2 \text{ m s}^{-1}$ . Other examples can be found in Fig. 10, where velocity offsets  $\Delta V$  of molecular pairs consistent with a single-component Gaussian model are depicted.

Some of our targets were partially mapped as indicated in Fig. 10. The six points of TMC-1C are scattered between  $\Delta V = -7 \pm 4 \text{ m s}^{-1}$  and  $104 \pm 2 \text{ m s}^{-1}$ , which is indicative of large systematic shifts caused by bulk motions. Indeed, the line widths of  $\text{NH}_3$  and  $\text{HC}_3\text{N}$  demonstrate the dominant influence of the non-thermal component. The measured ratio  $\beta = b(\text{NH}_3)/b(\text{HC}_3\text{N})$  at these points is equal to 1.0, 0.8, 1.2, 1.0, 1.2, and 1.0 at, respectively,  $(\Delta\alpha, \Delta\delta) = (0, 0), (0, -40), (0, 40), (-120, 90), (-60, 45),$  and  $(60, -45)$  arcsec. Similar velocity offsets are observed for L1495 and L183. In general, the scatter for the whole sample covers the range  $-100 \lesssim \Delta V \lesssim 100 \text{ m s}^{-1}$ . However, the scatter for the subsample selected in accord with the additional selection criteria from Sect. 5 decreases considerably. The corresponding points shown in Fig. 11 are distributed across the interval from  $-10$  to  $43 \text{ m s}^{-1}$ . Thus, as expected, molecular cores with thermally dominated gas motions are the most suitable targets for precise measurements of  $\Delta\mu/\mu$ .

It is essential that the observed spectral-line displacements are based on differential measurements of radial velocities recorded at the *same* telescope over short periods of time. It is also important that different receivers used in these observations enable the independent Doppler tracking of the observed molecular lines. Thus, there is no need for an accurate definition of the zero point, and only internal precisions of the measured line positions and the uncertainties in the rest-frame frequencies restrict the accuracy of the measured velocity offset.

### 5.2. Comparison with previously obtained results

In our preliminary analysis (LMK), we used high quality radio spectra of molecular cores in lines of  $\text{NH}_3$  ( $J, K$ ) = (1, 1)

(23 GHz), CCS  $J_N = 2_1 - 1_0$  (22 GHz),  $\text{HC}_3\text{N}$   $J = 5 - 4$  (45 GHz), and  $\text{N}_2\text{H}^+$   $J = 1 - 0$  (93 GHz). The observations were carried out with the 100-m Green Bank Telescope (GBT) by Rosolowsky et al. (2008) for the Perseus molecular cloud, by Rathborne et al. (2008) for the Pipe Nebula, and with the Nobeyama 45-m telescope by Sakai et al. (2008) for infrared dark clouds (IRDCs).

The most accurate estimates were obtained from carefully selected subsamples of the  $\text{NH}_3/\text{CCS}$  pairs observed with high spectral resolution (FWHM =  $25 \text{ m s}^{-1}$ ) in the Perseus molecular cloud ( $n = 21$ ) and the Pipe Nebula ( $n = 8$ ):  $\Delta V = 52 \pm 7_{\text{stat}} \pm 14_{\text{sys}} \text{ m s}^{-1}$  and  $69 \pm 11_{\text{stat}} \pm 14_{\text{sys}} \text{ m s}^{-1}$ , respectively. The analysis of the  $n = 36$   $\text{NH}_3/\text{N}_2\text{H}^+$  pairs and  $n = 27$   $\text{NH}_3/\text{HC}_3\text{N}$  pairs observed at lower spectral resolution (FWHM =  $120\text{--}500 \text{ m s}^{-1}$ ) in the IRDCs inferred that  $\Delta V = 160 \pm 32_{\text{stat}} \pm 14_{\text{sys}} \text{ m s}^{-1}$  and  $120 \pm 37_{\text{stat}} \pm 31_{\text{sys}} \text{ m s}^{-1}$ , respectively. At the same time, the rotational-rotational velocity differences for the IRDCs did not show any significant offset:  $\Delta V = V(\text{N}_2\text{H}^+) - V(\text{HC}_3\text{N}) = -17 \pm 34 \text{ km s}^{-1}$ .

The physical properties of low-mass ( $M \lesssim 10M_\odot$ ) molecular cores observed with the GBT are similar to those analyzed in the present paper. However, the IRDCs are more massive objects ( $M \gtrsim 100M_\odot$ ) with high turbulent velocities ( $\sim 1\text{--}3 \text{ km s}^{-1}$ ). The IRDCs are also more distant clouds, which are located towards the Galactic center at distances of 2-5 kpc. The spectral resolution used in observations of the IRDCs does not allow us to resolve the hyperfine structure of the  $\text{HC}_3\text{N}$   $J = 5 - 4$  transition (Sakai et al. 2008). The spectra of the  $\text{HC}_3\text{N}$  lines were fitted to a single Gaussian function and the corresponding radial velocities were calculated based on a single hyperfine line  $J = 5 - 4, F = 5 - 4$  with the frequency 45490.3102(3) MHz taken from the JPL catalog<sup>6</sup>. As a result, a systematic shift related to unresolved hyperfine components was introduced. We also note that the JPL frequencies are systematically shifted with respect to the CDMS catalogue (Müller et al. 2005). The CDMS frequency of the  $J = 5 - 4, F = 5 - 4$  transition is, for example, 45490.3137(5) MHz. Thus, it seems plausible that the large offset,  $\Delta V \gtrsim 100 \text{ m s}^{-1}$ , deduced from the IRDCs is caused by the superposition of unaccounted systematic shifts.

As for the low-mass cores in the Perseus molecular cloud and the Pipe Nebula, the discrepancy between our present estimate,  $\Delta V \simeq 20 \text{ m s}^{-1}$ , and the previously obtained value,  $\Delta V \simeq 60 \text{ m s}^{-1}$ , is probably caused by uncertainties in the rest-frame frequency of the CCS  $J_N = 2_1 - 1_0$  transition. In particular, the frequency 22344.033(1) MHz of this transition (used by both Rosolowsky et al. and Rathborne et al.) was calculated by comparing with the  $\text{HC}_3\text{N}$   $J = 5 - 4$  line observed towards a cold dark cloud L1498 assuming that (i) CCS and  $\text{HC}_3\text{N}$  are co-spatially distributed and (ii) the rest-frame frequency of  $\text{HC}_3\text{N}$   $J = 5 - 4, F = 5 - 4$  is 45490.316(1) MHz (Yamamoto et al. 1990). If the  $\text{HC}_3\text{N}$  frequency is 2 kHz lower as indicated in the CDMS catalogue, then the laboratory frequency of CCS decreases by 1 kHz, where 1 kHz at 22.3 GHz corresponds to  $13.4 \text{ m s}^{-1}$ , i.e., the difference  $V(\text{CCS}) - V(\text{NH}_3)$  becomes equal to  $\simeq 46 \text{ m s}^{-1}$ . The only known laboratory measurement of the CCS frequency infers, however, that 22344.029(4) MHz (Lovas et al. 1992). With this value  $V(\text{CCS}) - V(\text{NH}_3) \simeq 6 \text{ m s}^{-1}$ , but its error reaches

<sup>6</sup> <http://spec.jpl.nasa.gov>



53 m s<sup>-1</sup> (4 kHz at 22.3 GHz). The rest-frame frequency of CCS reported in the CDMS is 22344.0308(10) MHz. With this frequency, we obtain for the Perseus molecular cloud the offset  $\Delta V = 22 \pm 7_{\text{stat}} \pm 14_{\text{sys}}$  m s<sup>-1</sup>, which is in full agreement with our present estimate,  $\Delta V = 23 \pm 4_{\text{stat}} \pm 3_{\text{sys}}$  m s<sup>-1</sup>. This consideration makes it quite obvious that to increase the reliability of the results obtained, high precision laboratory measurements of molecular transition frequencies are badly needed.

## 6. Conclusions and future prospects

Using the 32-m Medicina, 100-m Effelsberg, and 45-m Nobeyama radio telescopes, we have performed precise spectral measurements of the relative radial velocity differences between the rotational transitions in HC<sub>3</sub>N ( $J = 2 - 1$ ) and N<sub>2</sub>H<sup>+</sup> ( $J = 1 - 0$ ) and the inversion transition in NH<sub>3</sub> ( $J, K = (1, 1)$ ). We detect a velocity offset of  $\Delta V = 23 \pm 4_{\text{stat}} \pm 3_{\text{sys}}$  m s<sup>-1</sup> between the rotational and inversion lines observed in cold molecular cores with dominating thermal motion. We do not find any plausible systematic effects that could mimic an offset of about 20 m s<sup>-1</sup> between rotational and inversion transitions and would be regularly reproduced in observations of different cold molecular cores with different facilities. The measured positive offset is qualitatively consistent with our preliminary result,  $\Delta V \simeq 60$  m s<sup>-1</sup>, obtained on the basis of the GBT observations of Rosolowsky et al. (2008) and Rathborne et al. (2008) of the NH<sub>3</sub>/CCS pairs in molecular cores in the Perseus molecular cloud and the Pipe Nebula (LMK). However, the rest-frame frequency of the CCS  $J_N = 2_1 - 1_0$  transition is not well known, and before deciding whether the difference between the current and preliminary results is statistically significant or not, new high precision laboratory measurements of the CCS frequency should be carried out.

If we assume that the measured velocity offset is caused by the electron-to-proton mass ratio variation, then  $\Delta\mu/\mu = 22 \pm 4_{\text{stat}} \pm 3_{\text{sys}}$  ppb. To account for the conditions of the terrestrial laboratory experiments, the non-zero  $\Delta\mu$  would require chameleon-like scalar field models that predict a strong dependence of mass and coupling constant on the ambient matter density.

In any case, our estimate defines a strongest conservative upper limit to  $|\Delta\mu/\mu| \leq 3 \times 10^{-8}$ , which can be considered as a reference point at  $z = 0$ . We note that extragalactic molecular clouds have gas densities similar to those in the interstellar clouds of the Milky Way. Thus, the value of  $\Delta\mu/\mu$  in high- $z$  molecular systems is expected to be at the same level as in the interstellar clouds, i.e.,  $\Delta\mu/\mu \sim 10^{-8}$ , provided that no temporal dependence of the electron-to-proton mass ratio is present.

To be completely confident that the derived velocity shift is not caused by kinematic effects in the clouds but reflects the density-modulated variation of  $\Delta\mu/\mu$ , new high precision radio-astronomical observations are needed for a wider range of objects. These observations should also target different molecules (i.e., not NH<sub>3</sub>) with tunneling transitions sensitive to the changes in  $\mu$  and molecules with  $\Lambda$ -doublet lines that also exhibit enhanced sensitivity to variations in  $\mu$  and  $\alpha$  (Kozlov 2009).

For the molecular transitions in question, it is very important to measure their rest-frame frequencies with an accuracy of about 1 m s<sup>-1</sup> in laboratory experiments. In some

**Table 2.** Hyperfine components of the NH<sub>3</sub> ( $J, K = (1, 1)$ ) transition. The velocity offsets,  $v_i$ , are relative to 23.694495487 GHz. Data from Kukolich (1967) and Ho (1977). Shown in parentheses are  $1\sigma$  errors.

#	$F'_1$	$F'$	$F_1$	$F$	Weight	$v_i$ , m s <sup>-1</sup>
1	1	1.5	0	0.5	0.317	-19549.98(48)
	1	0.5	0	0.5	0.159	-19411.73(61)
2	1	1.5	2	2.5	0.357	-7815.25(63)
	1	1.5	2	1.5	0.040	-7372.80(75)
	1	0.5	2	1.5	0.198	-7233.48(58)
3	2	1.5	2	2.5	0.071	-250.92(60)
	1	1.5	1	1.5	0.198	-213.00(47)
	2	2.5	2	2.5	1.000	-132.38(47)
	1	0.5	1	1.5	0.040	-75.17(75)
	2	1.5	2	1.5	0.643	192.27(56)
	2	2.5	2	1.5	0.071	311.03(80)
	1	1.5	1	0.5	0.040	322.04(35)
4	1	0.5	1	0.5	0.079	460.41(46)
	2	1.5	1	1.5	0.040	7351.32(49)
	2	2.5	1	1.5	0.357	7469.67(73)
5	2	1.5	1	0.5	0.198	7886.69(72)
	0	0.5	1	1.5	0.317	19315.90(71)
	0	0.5	1	0.5	0.159	19851.27(35) <sup>†</sup>

<sup>†</sup>The error of 0.35 m s<sup>-1</sup> corresponds to the difference between theoretically predicted (Ho 1977) and astronomically determined (Rydbeck et al. 1977) frequencies.

**Table 3.** Hyperfine components of the HC<sub>3</sub>N  $J = 2 - 1$  transition. The velocity offsets,  $v_i$ , are relative to 18.19621694 GHz. Data from Lapinov (2008, private comm.) and Müller et al. (2005).

#	$F'$	$F$	Weight	$v_i$ , m s <sup>-1</sup>
1	1	1	0.333	-35548.77(2.82)
2	1	2	0.022	-14167.97(2.83)
3	3	2	1.867	-1540.96(2.82)
4	2	1	1.000	0.00(2.82)
5	1	0	0.444	17806.60(2.82)
6	2	2	0.333	21380.64(2.82)

cases the present uncertainties in the rest-frame frequencies are larger than the errors of radio-astronomical measurements, thus preventing unambiguous conclusions.

In addition, searches for variations in the fine-structure constant  $\alpha$  within the Milky Way disk using mid- and far-infrared fine-structure transitions in atoms and ions (Kozlov et al. 2008), or searches for variations in the combination of  $\alpha^2/\mu$  using the [C II]  $\lambda 158 \mu\text{m}$  line and CO rotational lines (Levshakov et al. 2008b), or the [C I]  $\lambda 609 \mu\text{m}$  line and low-lying rotational lines of <sup>13</sup>CO (Levshakov et al. 2009) would be of great importance for cross-checking these results.

*Acknowledgements.* We are grateful to the staffs of the Medicina, Effelsberg, and Nobeyama radio observatories for excellent supports in our observations. The authors thank Dieter Engels for assistance in observations at the Medicina 32-m telescope. The project has been supported by DFG Sonderforschungsbereich SFB 676 Teilprojekt C4 and by the RFBR grant No. 09-02-12223. S.A.L. is supported by the RFBR grant No. 09-02-00352-a, and by the Federal Agency for Science and Innovations grant NSh 2600.2008.2. A.V.L. is supported by the RFBR grant No. 08-02-92001 and by the Program IV.12/2.5 of the Physical Department of the RAS.

**Table 1.** Target list.

#	Source	R.A. (J2000.0)	Dec. (J2000.0)	$V_{lsr}$ (km s <sup>-1</sup> )	Obs. <sup>a</sup>	Molecules <sup>b</sup>	References <sup>c</sup>
1	L1355	02:53:12.1	+68:55:52	-3.7	<i>m, e</i>	NH <sub>3</sub>	14
2	NH3SRC8	03:25:26.3	+30:45:05	+4.1	<i>m, e, n</i>	NH <sub>3</sub> , N <sub>2</sub> H <sup>+</sup>	5
3	NH3SRC28	03:27:26.4	+29:51:08	+5.6	<i>e</i>	NH <sub>3</sub>	5
4	NH3SRC36	03:27:55.9	+30:06:18	+4.7	<i>m</i>	NH <sub>3</sub>	5
5	NH3SRC91	03:30:15.2	+30:23:39	+5.9	<i>m</i>	NH <sub>3</sub>	5
6	NH3SRC95	03:30:32.1	+30:26:19	+6.1	<i>m</i>	NH <sub>3</sub> , HC <sub>3</sub> N	5
7	NH3SRC97	03:30:50.5	+30:49:17	+7.7	<i>e</i>	NH <sub>3</sub>	5
8	L1489	04:04:49.0	+26:18:42	+6.7	<i>e, n</i>	NH <sub>3</sub> , HC <sub>3</sub> N, N <sub>2</sub> H <sup>+</sup>	1, 4
9	L1498	04:10:51.4	+25:09:58	+7.8	<i>e, n</i>	NH <sub>3</sub> , HC <sub>3</sub> N, N <sub>2</sub> H <sup>+</sup>	1, 3, 4, 6
10	L1495	04:14:08.2	+28:08:16	+6.8	<i>e, n</i>	NH <sub>3</sub> , HC <sub>3</sub> N, N <sub>2</sub> H <sup>+</sup>	1, 6
11	L1521F	04:28:39.8	+26:51:35	+6.5	<i>e</i>	NH <sub>3</sub> , HC <sub>3</sub> N	4, 6, 10
12	L1524	04:29:22.7	+24:34:58	+6.5	<i>e, n</i>	NH <sub>3</sub> , HC <sub>3</sub> N, N <sub>2</sub> H <sup>+</sup>	4, 8, 10
13	B217S-W	04:27:46.4	+26:17:52	+7.0	<i>e</i>	NH <sub>3</sub> , HC <sub>3</sub> N	1, 4, 12
14	L1400K	04:30:52.0	+54:51:55	+3.3	<i>e, n</i>	NH <sub>3</sub> , HC <sub>3</sub> N	1, 3, 4, 6
15	TMC-2	04:32:48.6	+24:25:12	+6.2	<i>e, n</i>	NH <sub>3</sub> , HC <sub>3</sub> N, N <sub>2</sub> H <sup>+</sup>	1
16	L1536	04:33:23.5	+22:42:46	+5.6	<i>e, n</i>	NH <sub>3</sub> , HC <sub>3</sub> N, N <sub>2</sub> H <sup>+</sup>	1, 4
17	CB22	04:40:33.1	+29:55:04	+6.0	<i>e</i>	NH <sub>3</sub> , HC <sub>3</sub> N	4
18	TMC-1C	04:41:38.8	+26:00:42	+5.2	<i>m, e, n</i>	NH <sub>3</sub> , HC <sub>3</sub> N, N <sub>2</sub> H <sup>+</sup>	1, 2, 3, 4
19	TMC-1/HC3N	04:41:41.8	+25:41:42	+5.9	<i>m</i>	NH <sub>3</sub> , HC <sub>3</sub> N	9, 11
20	CB23	04:43:27.7	+29:39:11	+6.0	<i>e, n</i>	NH <sub>3</sub> , HC <sub>3</sub> N, N <sub>2</sub> H <sup>+</sup>	4, 6
21	L1517B	04:55:18.8	+30:38:04	+5.8	<i>e, n</i>	NH <sub>3</sub> , HC <sub>3</sub> N, N <sub>2</sub> H <sup>+</sup>	2, 4, 6
22	L1512	05:04:09.6	+32:43:09	+7.1	<i>m, e, n</i>	NH <sub>3</sub> , HC <sub>3</sub> N, N <sub>2</sub> H <sup>+</sup>	1, 2, 4, 6, 8
23	L1544	05:04:16.5	+25:10:48	+7.2	<i>e, n</i>	NH <sub>3</sub> , HC <sub>3</sub> N	3, 4, 6, 8, 9
24	L134A	15:53:36.2	-04:35:26	+2.7	<i>e</i>	NH <sub>3</sub>	4, 6, 8
25	L183	15:54:06.4	-02:52:23	+2.4	<i>m, e, n</i>	NH <sub>3</sub> , HC <sub>3</sub> N, N <sub>2</sub> H <sup>+</sup>	4, 6, 7, 8
26	L43	16:34:35.0	-15:46:36	+0.7	<i>e, n</i>	NH <sub>3</sub> , HC <sub>3</sub> N, N <sub>2</sub> H <sup>+</sup>	4
27	L260-NH3	16:47:06.6	-09:35:21	+3.5	<i>e, n</i>	NH <sub>3</sub> , HC <sub>3</sub> N, N <sub>2</sub> H <sup>+</sup>	1, 8, 12
28	L234A	16:48:06.8	-10:51:48	+2.9	<i>e</i>	NH <sub>3</sub> , HC <sub>3</sub> N	4, 8
29	L234S-E	16:48:08.6	-10:57:25	+3.2	<i>e</i>	NH <sub>3</sub>	4
30	L63	16:50:15.4	-18:06:06	+5.7	<i>e</i>	NH <sub>3</sub> , HC <sub>3</sub> N	4, 8
31	CB68	16:57:19.4	-16:09:25	+5.2	<i>e</i>	NH <sub>3</sub> , HC <sub>3</sub> N	4
32	L492	18:15:49.6	-03:46:14	+7.7	<i>e</i>	NH <sub>3</sub> , HC <sub>3</sub> N	6
33	L778	19:26:32.5	+23:58:42	+9.9	<i>m</i>	NH <sub>3</sub>	1, 4
34	B335	19:37:01.3	+07:34:07	+8.4	<i>e</i>	NH <sub>3</sub> , HC <sub>3</sub> N	4, 8
35	L694-2	19:41:04.4	+10:57:02	+9.5	<i>m, e</i>	NH <sub>3</sub>	6, 13
36	L1049-2	20:41:30.5	+57:33:44	+0.1	<i>e</i>	NH <sub>3</sub>	15
37	L1251T3	22:29:50.3	+75:13:25	-3.8	<i>e, n</i>	NH <sub>3</sub> , HC <sub>3</sub> N, N <sub>2</sub> H <sup>+</sup>	4
38	L1251T2	22:30:31.2	+75:13:38	-4.0	<i>e, n</i>	NH <sub>3</sub> , HC <sub>3</sub> N, N <sub>2</sub> H <sup>+</sup>	4
39	L1251T1	22:31:02.3	+75:13:39	-4.2	<i>e, n</i>	NH <sub>3</sub> , HC <sub>3</sub> N, N <sub>2</sub> H <sup>+</sup>	4
40	L1251C	22:35:53.6	+75:18:55	-4.7	<i>e, n</i>	NH <sub>3</sub> , HC <sub>3</sub> N, N <sub>2</sub> H <sup>+</sup>	16, 17
41	L1197	22:37:02.1	+58:57:22	-3.1	<i>e, n</i>	NH <sub>3</sub> , HC <sub>3</sub> N, N <sub>2</sub> H <sup>+</sup>	6, 13

<sup>a</sup> Observations: *m* – Medicina 32-m, *e* – Effelsberg 100-m, and *n* – Nobeyama 45-m radio telescopes.

<sup>b</sup> Detected transitions: NH<sub>3</sub> ( $J, K$ ) = (1, 1), HC<sub>3</sub>N  $J = 2 - 1$ , N<sub>2</sub>H<sup>+</sup>  $J = 1 - 0$ .

<sup>c</sup> References: (1) Benson & Myers 1989; (2) Myers et al. 1983; (3) Howe et al. 1994; (4) Jijina et al. 1999; (5) Rosolowsky et al. 2008; (6) Crapsi et al. 2005; (7) Pagani et al. 2009; (8) Fuller & Myers 1993; (9) Churchwell et al. 1984; (10) Codella et al. 1997; (11) Benson & Myers 1983; (12) Motte & Andre 2001; (13) Lee et al. 2007; (14) Park et al. 2004; (15) Lee et al. 1999; (16) Caselli et al. 2002; (17) Walsh et al. 2004.

## Appendix A: Robust statistics

A comprehensive review of robust statistical procedures is given by Hampel et al. (1986) (see also Chap. 15.7 in Press et al. 1992).

Robust estimates are insensitive to departures of the distribution shape from the assumed data distribution. In particular,  $M$ -estimates (maximum-likelihood) are usually relevant for the estimate of parameters with continuous distributions. The shift (mean),  $m$ , and the scale (standard deviation),  $s$ , of a sample of data points  $\{x_i\}$  are estimated by minimizing the sum  $\sum_i \Psi[(x_i - m)/s]$ . Here  $\Psi$  is a weighting function such that the weights given to individual points

first increase with deviations from  $m$ , and then decrease so that very outlying points (outliers) are not counted at all (re-descending  $M$ -estimate). The following functions are prescribed for use as  $\Psi$ :

Hampel's function

$$\Psi(u) = \text{sign}(u) \begin{cases} |u|, & 0 \leq |u| \leq 1.7 \\ 1.7, & 1.7 \leq |u| \leq 3.4 \\ \frac{8.5 - |u|}{3}, & 3.4 \leq |u| \leq 8.5 \\ 0, & u > 8.5 \end{cases}$$

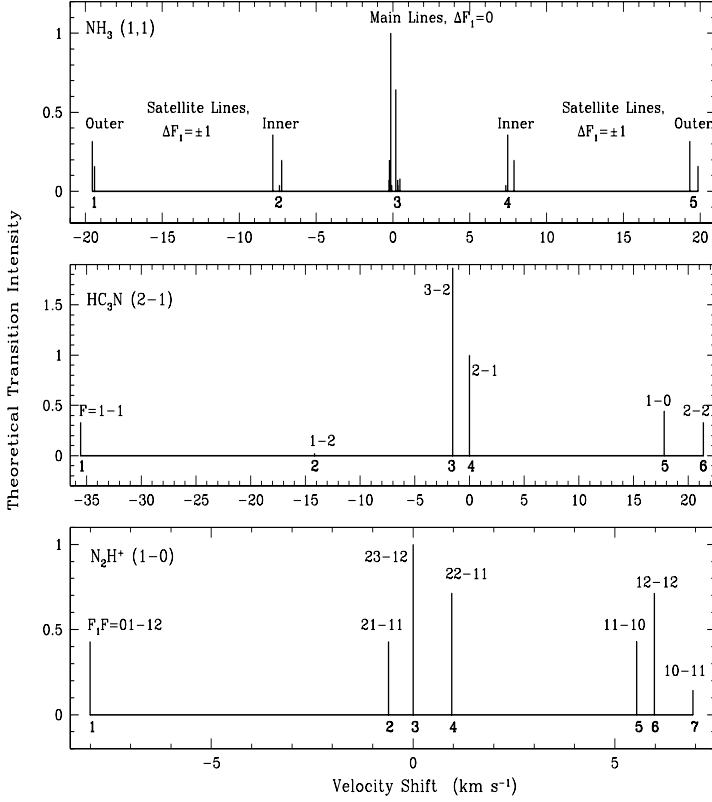


**Fig. 1.** Sketch of the hyperfine transitions for the  $\text{NH}_3$  (1,1),  $\text{HC}_3\text{N}$  (2 – 1), and  $\text{N}_2\text{H}^+$  (1 – 0) states. Line identification numbers are given in each panel (see Tables 2 – 4).

**Table 4.** Hyperfine components of the  $\text{N}_2\text{H}^+$   $J = 1 - 0$  transition. The velocity offsets,  $v_i$ , are relative to 93.1737722 GHz. Data from Müller et al. (2005).

#	$F'_1$	$F'$	$F_1$	$F$	Weight	$v_i$ , m s $^{-1}$
1	0	1	1	0	0.076	–8008.2(13.8)
	0	1	1	1	0.100	–8008.2(13.8)
	0	1	1	2	0.252	–8008.2(13.8)
2	2	1	1	2	0.017	–622.6(13.8)
	2	1	1	0	0.134	–622.6(13.8)
	2	1	1	1	0.278	–622.6(13.8)
3	2	3	1	2	1.000	0.00(13.2)
4	2	2	1	2	0.111	956.9(13.5)
	2	2	1	1	0.604	956.9(13.5)
5	1	1	1	1	0.051	5541.6(13.5)
	1	1	1	2	0.159	5541.6(13.5)
	1	1	1	0	0.218	5541.6(13.5)
6	1	2	1	1	0.111	5982.4(13.5)
	1	2	1	2	0.604	5982.4(13.5)
7	1	0	1	1	0.143	6934.2(13.2)

Andrew’s sine

$$\Psi(u) = \begin{cases} \sin\left(\frac{u}{c}\right), & |u| < c\pi \\ 0, & |u| > c\pi \end{cases}$$

optimal value for  $c = 2.1$ , and  
Tukey’s biweight

$$\Psi(u) = \begin{cases} u\left(1 - \frac{u^2}{c^2}\right)^2, & |u| < c \\ 0, & |u| > c \end{cases}$$

optimal value for  $c = 5 - 6$ .

The minimization occurs iteratively, the initial guess for  $m$  being the median of the data set, and for the scale  $s$  the normalized median absolute deviation ( $1.48 \cdot \text{MAD}$ ). All estimations presented in the paper were obtained with Tukey’s biweight. Other  $\Psi$ -functions provide similar results.

## References

- Benson, P. J., & Myers, P. C. 1989, *ApJS*, 71, 89  
 Benson, P. J., & Myers, P. C. 1983, *ApJ*, 270, 589  
 Blatt, S., Ludlow, A. D., Campbell, G. K., et al. 2008, *Phys. Rev. Lett.*, 100, 140801  
 Brax, P., van de Bruck, C., Davis, A.-C., Khoury, J., & Weltman, A. 2004, *Phys. Rev. D*, 70, 123518  
 Burrage, C., Davis, A.-C., & Shaw, D. J. 2009, *Phys. Rev. D*, 79, 044028  
 Caldwell, R. R., Dave, R., & Steinhardt, P. J. 1998, *Phys. Rev. Lett.*, 80, 1582  
 Calmet, X., & Fritzsche, H. 2002, *Eur. Phys. J. C*, 24, 639  
 Caselli, P., Benson, P. J., Meyers, P. S., & Thaddeus, P. 2002, *ApJ*, 572, 238  
 Caselli, P., Meyers, P. S., & Thaddeus, P. 1995, *ApJ*, 455, L77  
 Chand, H., Srianand, R., Petitjean, P., & Aracil, B. 2004, *A&A*, 417, 853  
 Churchwell, E., Nash, A. G., & Walmsley, C. M. 1984, *ApJ*, 287, 681  
 Codella, C., Welser, R., Henkel, C., Benson, P. J., & Myers, P. C. 1997, *A&A*, 324, 203  
 Crapsi, A., Caselli, P., Walmsley, C. M., et al. 2005, *ApJ*, 619, 379  
 Daniel, F., Cernicharo, J., Roueff, E., Gerin, M., & Dubernet, M. L. 2007, *ApJ*, 667, 980  
 Davis, A.-C., Schelpe, C. A. O., & Shaw, D. J. 2009, *Phys. Rev. D*, 80, 064016  
 Di Francesco, J., Evans, N. J., II, Caselli, P., et al. 2007, in *Protostars and Planets. V.*, eds. B. Reipurth, D. Jewitt, and K. Keil (Uni. Arizona Press, Tucson), p. 17

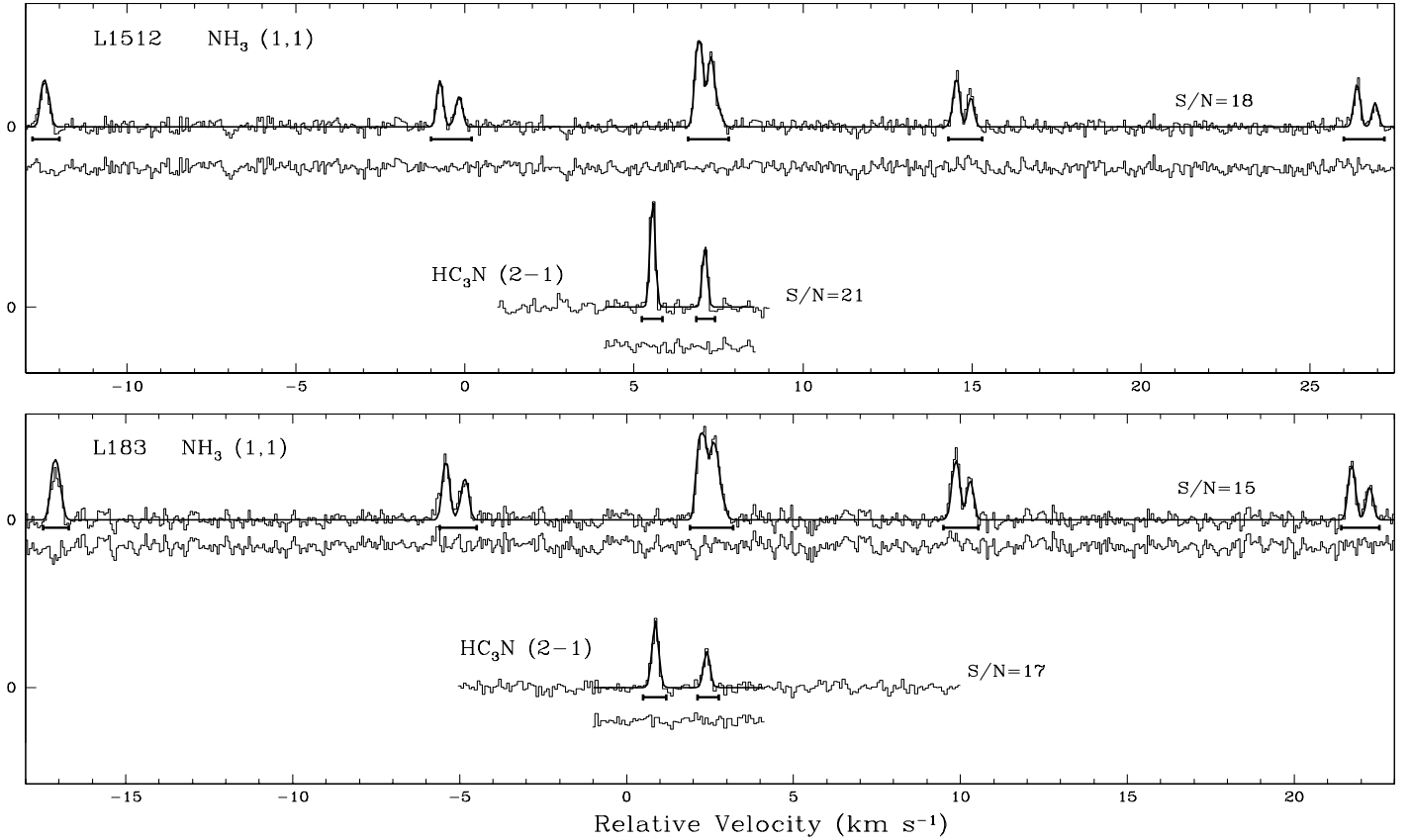


**Fig. 2.** Spectra of  $\text{NH}_3$  (1,1) and  $\text{HC}_3\text{N}$  (2 – 1) toward the cores L1512 and L183 obtained at the Medicina 32-m radio telescope. The histogram shows the data, the solid curve shows the fit, and the residual is plotted below each profile. The horizontal thick bars mark spectral windows used in the fitting procedure. The data are the arithmetic means of all the observations. The size of the resolution element (pixel) is  $62 \text{ m s}^{-1}$  for  $\text{NH}_3$ , and  $80 \text{ m s}^{-1}$  for  $\text{HC}_3\text{N}$ . For each spectrum, the signal-to-noise ratio (S/N) per pixel at the maximum intensity peak is depicted.

- Dickman, R. L. 1975, *ApJ*, 202, 50  
Dine, M., Nir, Y., Raz, G., & Volansky, T. 2003, *Phys. Rev. D*, 67, 015009  
Flambaum, V. V., & Kozlov, M. G. 2007, *Phys. Rev. Lett.*, 98, 240801  
Flambaum, V. V., Leinweber, D. B., Thomas, A. W., & Young, R. D. 2004, *Phys. Rev. D*, 69, 115006  
Flower, D. R., Pineau des Forêts, G., & Walmsley, C. M. 2006, *A&A*, 456, 215  
Fuller, G. A., & Myers, P. C. 1993, *ApJ*, 418, 273  
Griest, K., Whitmore, J. B., Wolfe, A. M., et al. 2010, *ApJ*, 708, 158  
Hampel, F. R., Ronchetti, E. M., Rousseeuw, P. J., & Stahel, W. A. 1986, *Robust Statistics. The Approach Based on Influence Functions* (John Wiley & Sons: N.Y.)  
Henkel, C., Menten, K. M., Murphy, M. T., et al. 2009, *A&A*, 500, 725  
Ho, P. T. P. 1977, Ph. D. thesis, Massachusetts Institute of Technology  
Ho, P. T. P., & Townes, C. H. 1983, *ARA&A*, 21, 239  
Hotzel, S., Harju, J., & Walmsley, C. M. 2004, *A&A*, 415, 1065  
Hougen, J. T. 1972, *J. Chem. Phys.*, 57, 4207  
Howe, D. A., Millar, T. J., Schilke, P., & Walmsley, C. M. 1994, *MNRAS*, 267, 59  
Jijina, J., Hyers, P. C., & Adams, F. C. 1999, *ApJS*, 125, 161  
Khoury, J., & Weltman, A. 2004, *Phys. Rev. Lett.*, 93, 171104  
King, J. A., Webb, J. K., Murphy, M. T., & Carswell, R. F. 2008, *Phys. Rev. Lett.*, 101, 251304  
Kozlov, M. G. 2009, *Phys. Rev. A*, 80, 022118  
Kozlov, M. G., Porsev, S. G., Levshakov, S. A., Reimers, D., & Molaro, P. 2008, *Phys. Rev. A*, 77, 032119  
Kukolich, S. G. 1967, *Phys. Rev.*, 156, 83  
Langacker, P., Segrè, G., & Strassler, M. J. *Phys. Lett. B*, 528, 121  
Lapinov, A. V., in *15th Symp. on High-Resolution Molecular Spectroscopy*, eds. Y. N. Ponomarev, S. N. Mikhailenko, and L. N. Sinita, 2006, *Proceed. of SPIE*, 6580, 658001  
Lee, C. W., Myers, P. C., & Tafalla, M. 1999, *ApJ*, 526, 788  
Lee, H.-H., Herbst, E., Pineau des Forêts, G., Roueff, F., Le Bourlot, J. 1996, *A&A*, 311, 690  
Lee, S. H., Park, Y.-S., Sohn, J., Lee, C. W., & Lee, H. M. 2007, *ApJ*, 660, 1326  
Levshakov, S. A., Molaro, P., & Reimers, D. 2009, *A&A*, submitted  
Levshakov, S. A., Molaro, P., & Kozlov, M. G. 2008a, arXiv: astro-ph/0808.0583 [LMK]  
Levshakov, S. A., Reimers, D., Kozlov, M. G., Porsev, S. G., & Molaro, P. 2008b, *A&A*, 479, 719  
Levshakov, S. A., Molaro, P., Lopez, S., et al. 2007, *A&A*, 466, 1077  
Levshakov, S. A., Centurión, M., Molaro, P., & D’Odorico, S. 2005, *A&A*, 434, 827  
Levshakov, S. A., Dessauges-Zavadsky, M., D’Odorico, S., & Molaro, P. 2002, *MNRAS*, 333, 373  
Lovas, F. J., Suenram, R. D., Ogata, T., & Yamamoto, S. 1992, *ApJ*, 399, 325  
Myers, P. C., Linke, R. A., & Benson, P. J. 1983, *ApJ*, 264, 517  
Molaro, P., Levshakov, S. A., & Kozlov, M. G. 2009, *Nucl. Phys. Proc. Suppl.*, 194, 287 (astro-ph/0907.1192)  
Molaro, P., Reimers, D., Agafonova, I. I., & Levshakov, S. A. 2008, *EPJST*, 163, 173  
Mota, D. F., & Shaw, D. J. 2007, *Phys. Rev. D*, 75, 063501  
Mota, D. F., & Barrow, J. D. 2004, *MNRAS*, 349, 291  
Motte, F., & André, P. 2001, *A&A*, 365, 440  
Müller, H. S. P., Schlöder, F., Stutzki, J., & Winnewisser, G. 2005, *J. Mol. Struct.*, 742, 215  
Murphy, M. T., Webb, J. K., & Flambaum, V. V. 2008a, *MNRAS*, 384, 1053

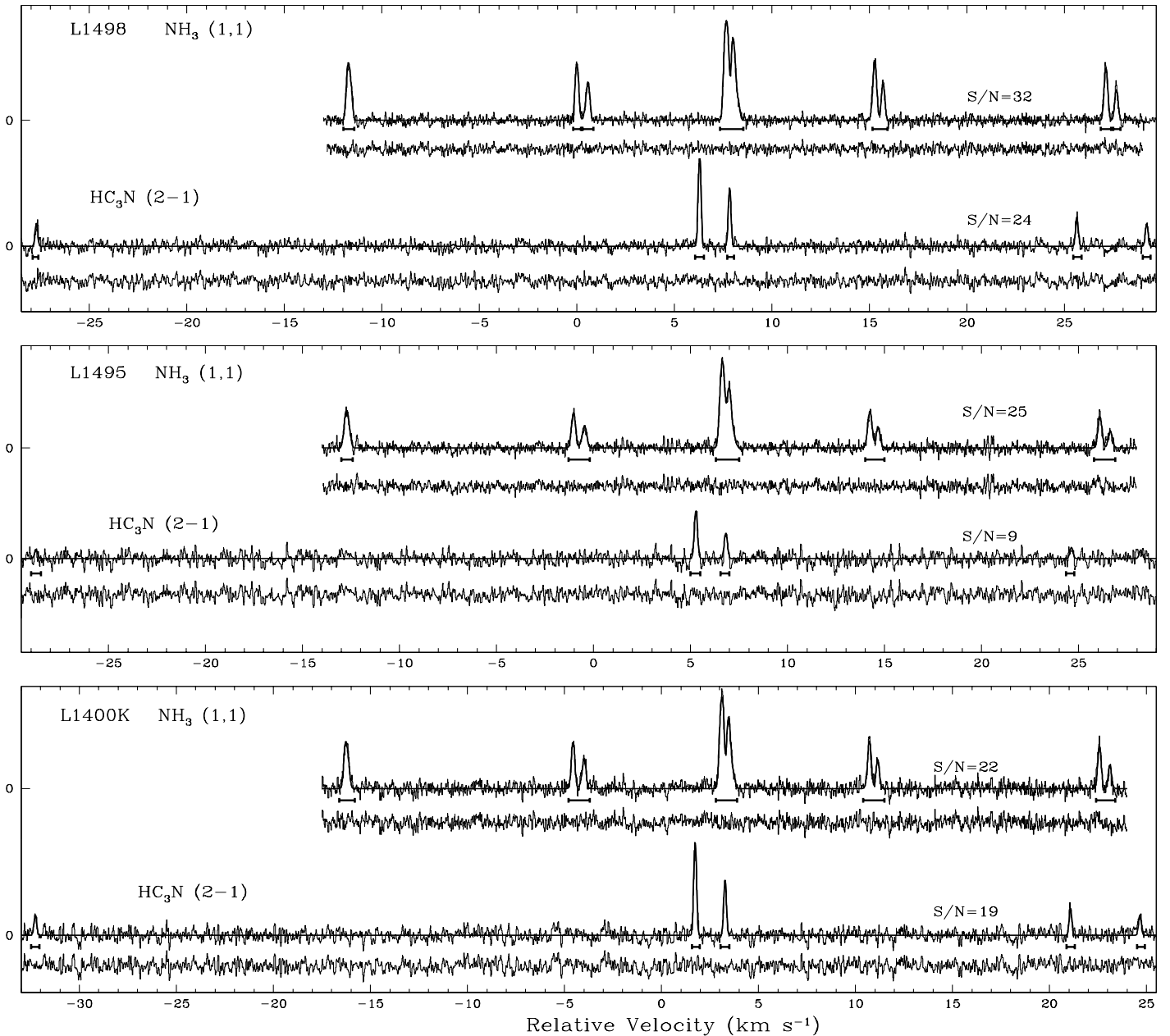


**Fig. 3.** Spectra of  $\text{NH}_3$  (1,1) and  $\text{HC}_3\text{N}$  (2 – 1) toward the cores L1498, L1495, and L1400K obtained at the Effelsberg 100-m radio telescope. The histogram shows the data, the solid curve shows the fit, and the residual is plotted below each profile. The horizontal thick bars mark spectral windows used in the fitting procedure. The data are the arithmetic means of all the observations. The size of the resolution element (pixel) is  $15 \text{ m s}^{-1}$  for  $\text{NH}_3$ , and  $20 \text{ m s}^{-1}$  for  $\text{HC}_3\text{N}$ . For each spectrum, the signal-to-noise ratio (S/N) per pixel at the maximum intensity peak is depicted.

Murphy, M. T., Flambaum, V. V., Muller, S., & Henkel, C. 2008b, *Science*, 320, 1611  
 Murphy, M. T., Flambaum, V. V., Webb, J. K., et al. 2004, *Lect. Notes Phys.*, 648, 131  
 Nakajima, T., Sakai, T., Asayama, S., et al. 2008, *PASJ*, 60, 435  
 Olano, C. A., Walmsley, C. M., & Wilson, T. L. 1988, *A&A*, 196, 194  
 Olive, K. A., & Pospelov, M. 2008, *Phys. Rev. D*, 77, 043524  
 Pagani, L., Daniel, F., & Dubernet, M.-L. 2009, *A&A*, 494, 719  
 Park, Y.-S., Lee, C. W., & Myers, P. C. 2004, *ApJS*, 152, 81  
 Peebles, P. J. E., & Rata, B. 2003, *Rev. Mod. Phys.*, 75, 559  
 Press, W. H., Teukolsky, S. A., Vetterling, W. T., & Flannery, B. P. 1992, *Numerical Recipes in C* (Cambridge: Cambridge Uni. Press)  
 Quast, R., Reimers, D., & Levshakov, S. A. 2004, *A&A*, 415, L7  
 Rathborne, J. M., Lada, C. J., Muench, A. A., Alves, J. F., & Lombardi, M. 2008, *ApJS*, 174, 396

Reinhold, E., Buning, R., Hollenstein, U., et al. 2006, *Phys. Rev. Lett.*, 96, 151101  
 Rosenband, T., Hume, D. B., Schmidt, P. O., et al. 2008, *Science*, 319, 1808  
 Rosolowsky, E. W., Pineda, J. E., Foster, J. B., et al. 2008, *ApJS*, 175, 509  
 Rydbeck, O. E. H., Sume, A., Hjalmarsen, A., et al. 1977, *ApJ*, 215, L35  
 Sakai, T., Sakai, N., Kamegai, K., et al. 2008, *ApJ*, 678, 1049  
 Shelkownikov, A., Butcher, R. J., Chardonnet, C., & Amy-Klein, A. 2008, *Phys. Rev. Lett.*, 100, 150801  
 Srianand, R., Chand, H., Petitjean, P., & Aracil, B. 2008, *Phys. Rev. Lett.*, 100, 029902  
 Stuart, A., & Ord, K. 1994, *Kendall's Advanced Theory of Statistics*, vol. I (Hodder Arnild: London)  
 Suzuki, H., Yamamoto, S., Ohishi, M., et al. 1992, *ApJ*, 392, 551

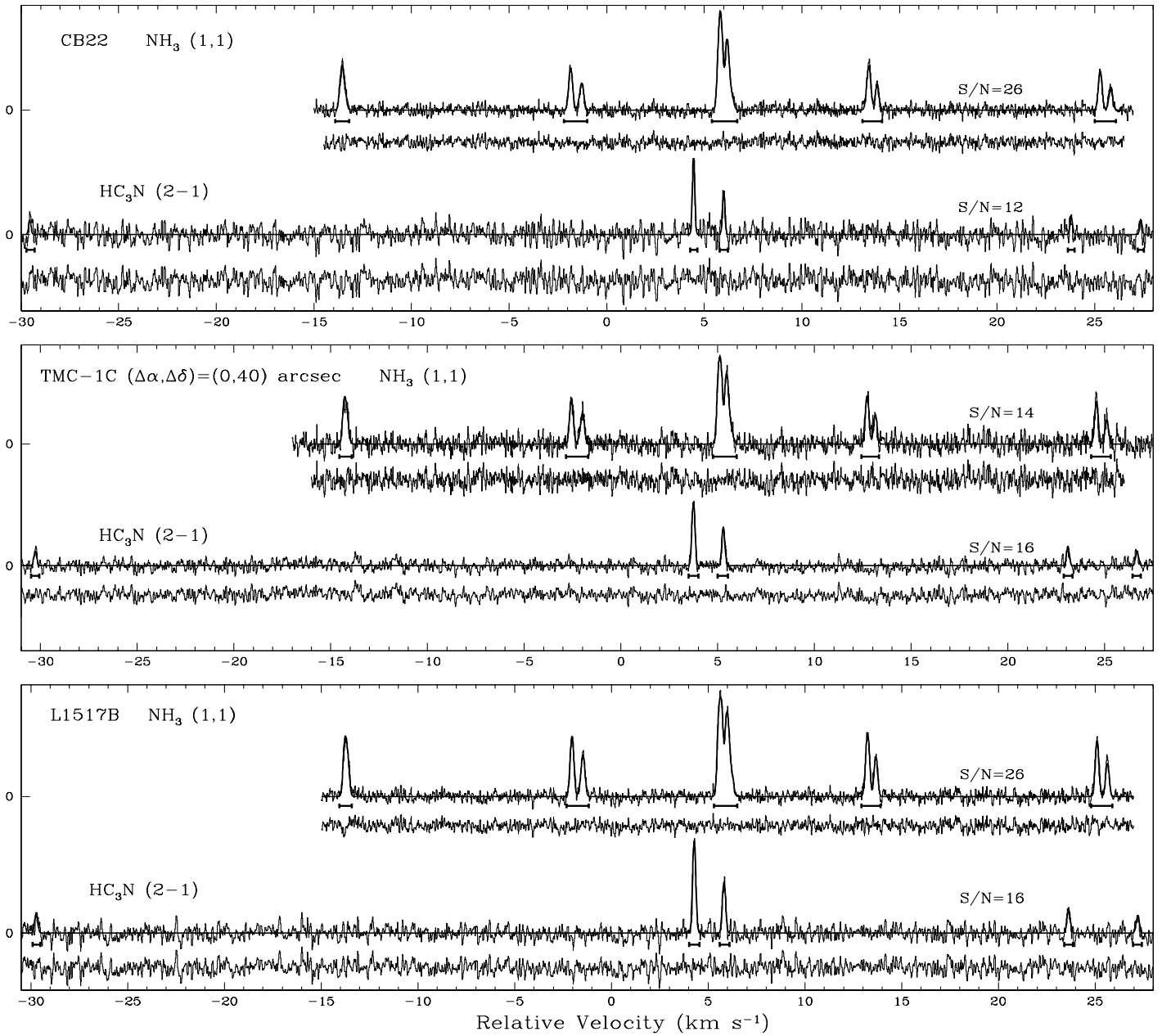


**Fig. 4.** Same as Fig. 3 but for the cores CB22, TMC-1C (offset  $\Delta\alpha, \Delta\delta = 0, 40$  arcsec), and L1517B.

- Tafalla, M., Myers, P. C., Caselli, P., & Walmsley, C. M. 2004, *A&A*, 416, 191  
 Thompson, R. I., Bechtold, J., Black, J. H., et al. 2009, *ApJ*, 703, 1648  
 Thompson, R. I. 1975, *Astrophys. Lett.*, 16, 3  
 van Veldhoven, J., Küpper, J., Bethlem, H. L., et al. 2004, *Eur. Phys. J. D*, 31, 337  
 Varshalovich, D. A., & Levshakov, S. A. 1993, *J. Exp. Theor. Phys. Lett.*, 58, 237  
 Walmsley, C. M., & Ungerechts, H. 1983, *A&A*, 122, 164  
 Walsh, A. J., Myers, P. C., & Burton, M. C. 2004, *ApJ*, 614, 194  
 Wendt, M., & Reimers, D. 2008, *EPJST*, 163, 197  
 Yamamoto, S., Saito, S., Kawaguchi, K., & Ohishi, M. 1990, *ApJ*, 361, 318

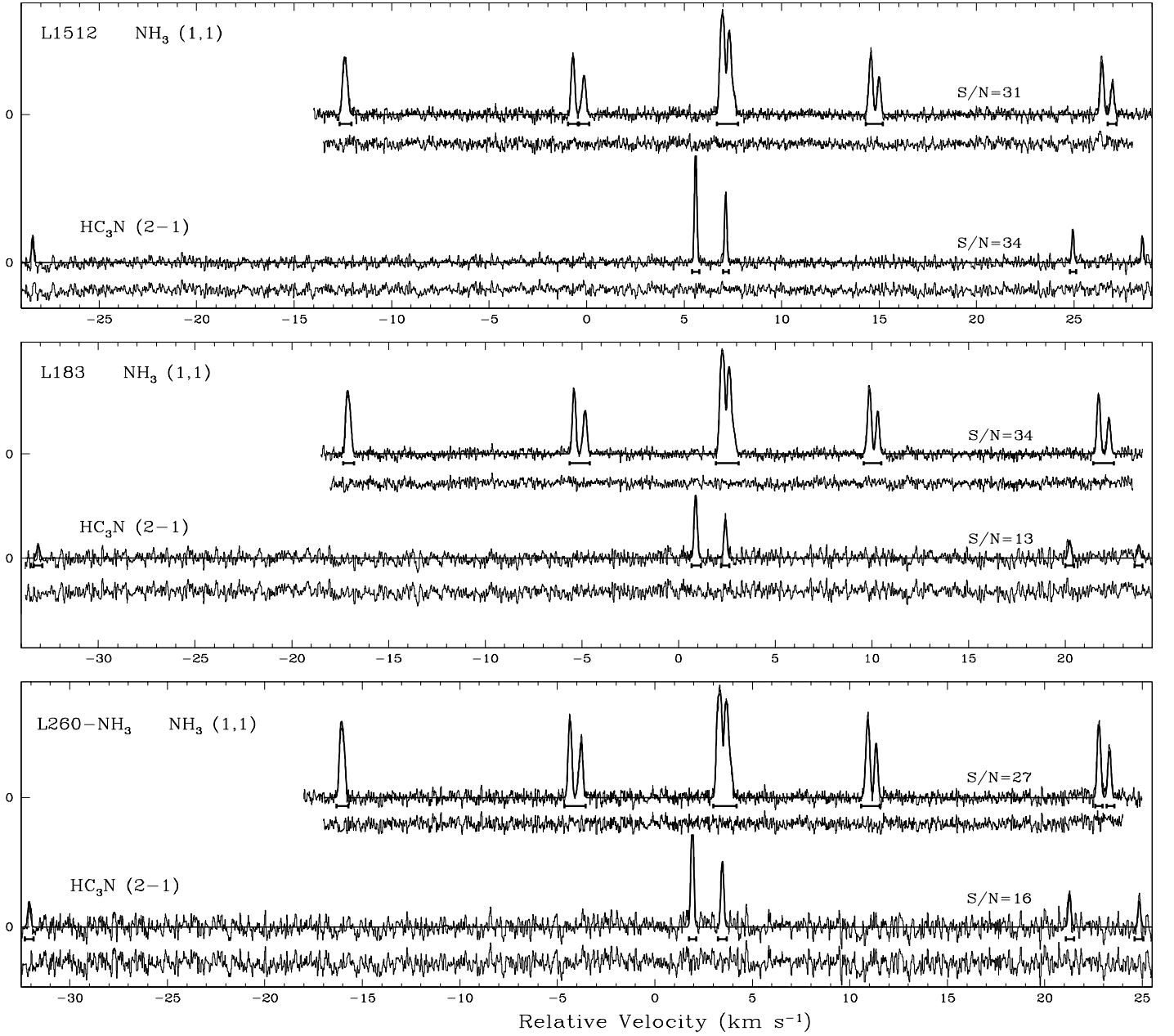
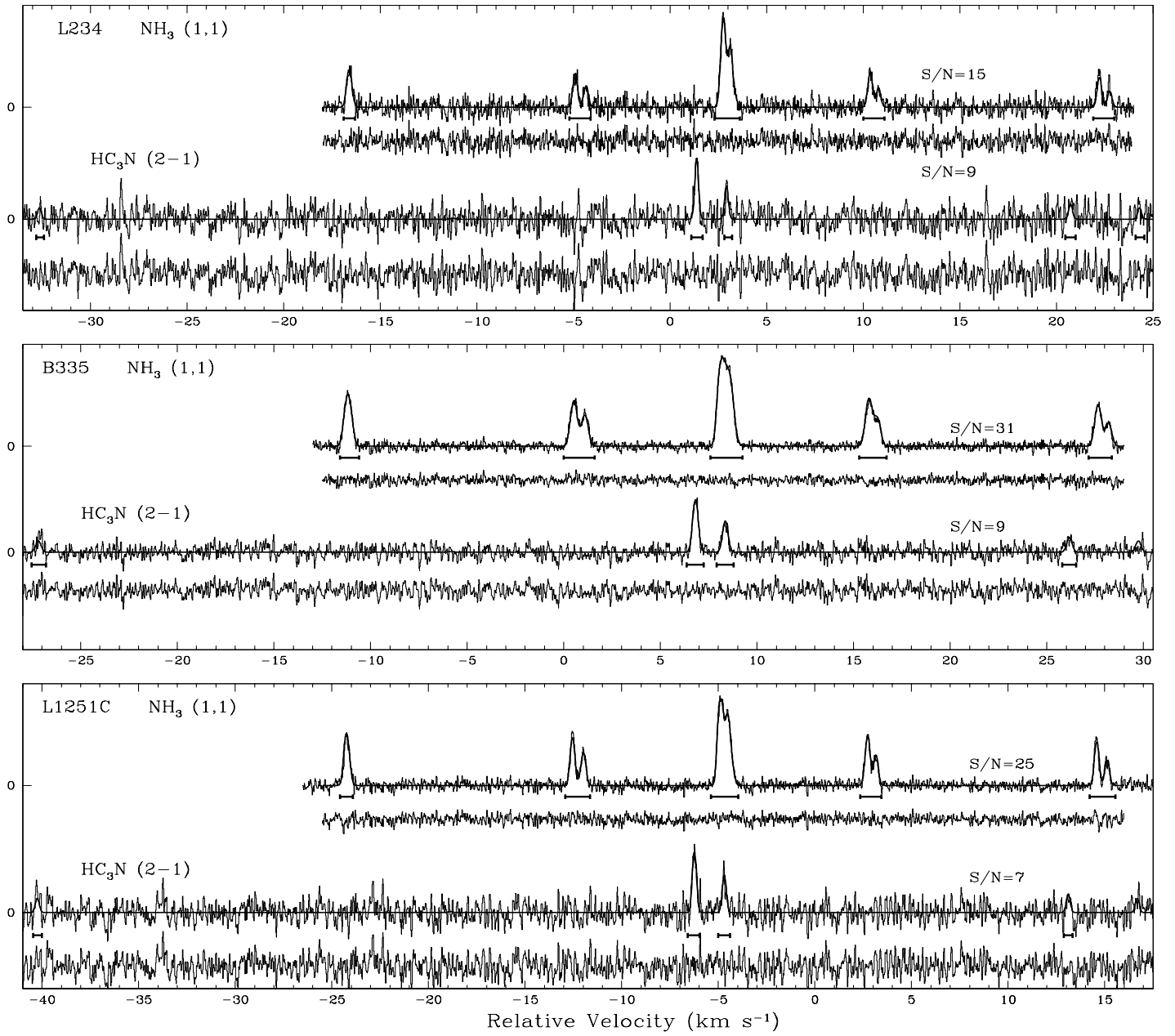
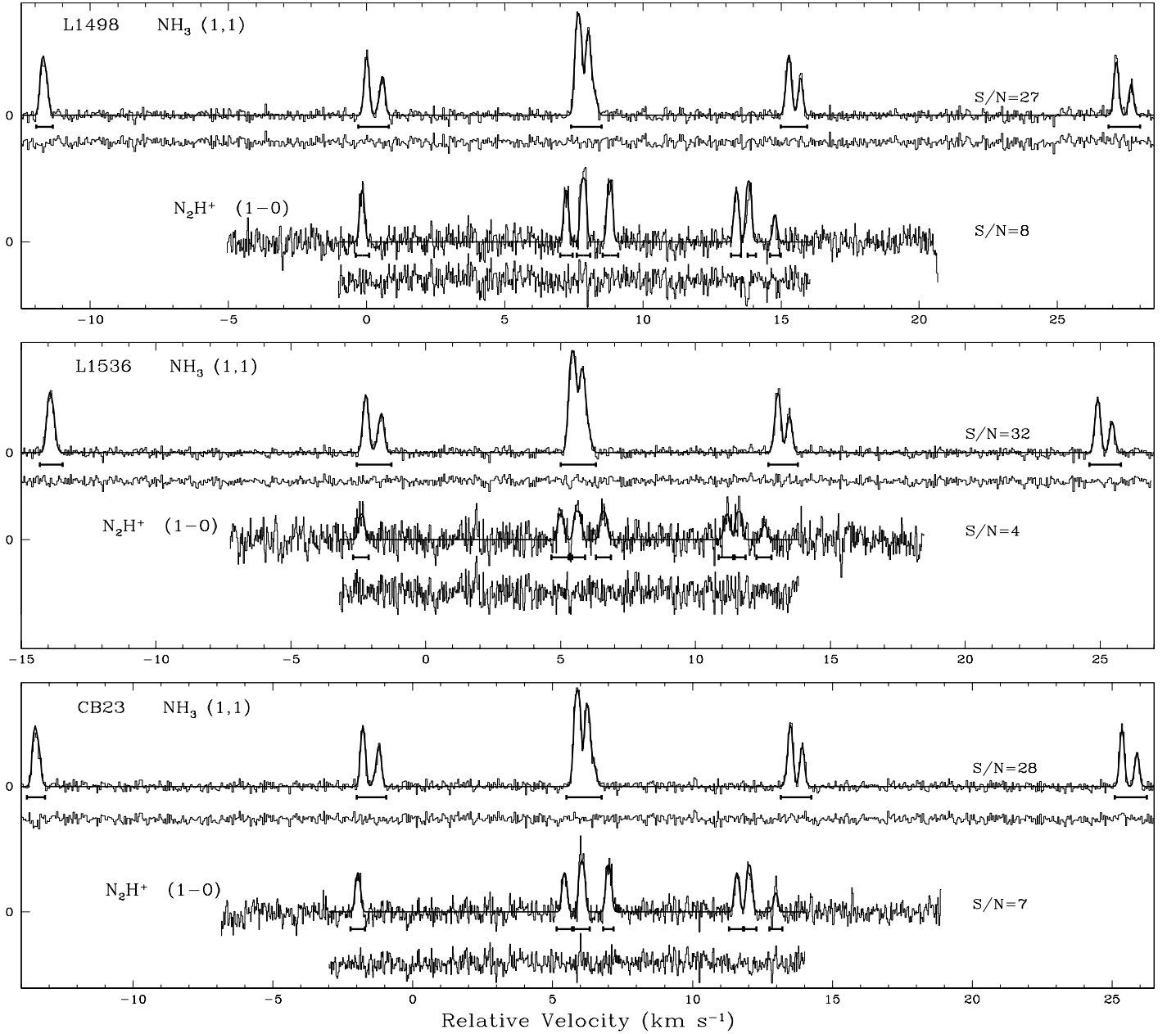


Fig. 5. Same as Fig. 3 but for the cores L1512, L183, and L260-NH<sub>3</sub>.



**Fig. 6.** Same as Fig. 3 but for the cores L234A, B335, and L1251C.





**Fig. 7.** Spectra of  $\text{NH}_3$  (1,1) and  $\text{N}_2\text{H}^+$  (1-0) toward the cores L1498, L1536, and CB23 obtained at the Nobeyama 45-m radio telescope. The histogram shows the data, the solid curve shows the fit, and the residual is plotted below each profile. The horizontal thick bars mark spectral windows used in the fitting procedure. The data are the arithmetic means of all the observations. The size of the resolution element (pixel) is  $49 \text{ m s}^{-1}$  for  $\text{NH}_3$ , and  $25 \text{ m s}^{-1}$  for  $\text{N}_2\text{H}^+$ . For each spectrum, the signal-to-noise ratio (S/N) per pixel at the maximum intensity peak is depicted.

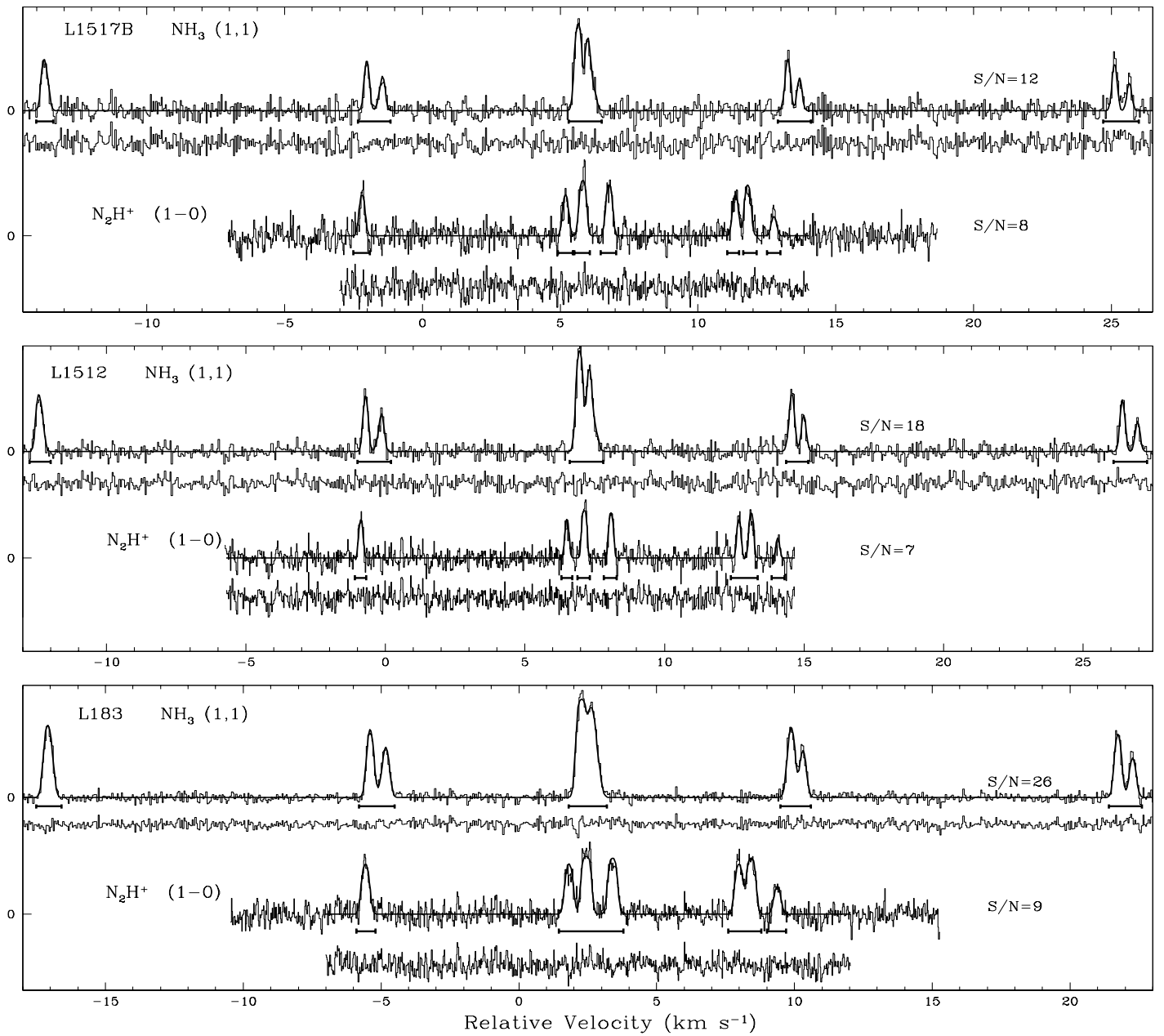


**Fig. 8.** Same as Fig. 7 but for the cores L1517B, L1512, and L183.

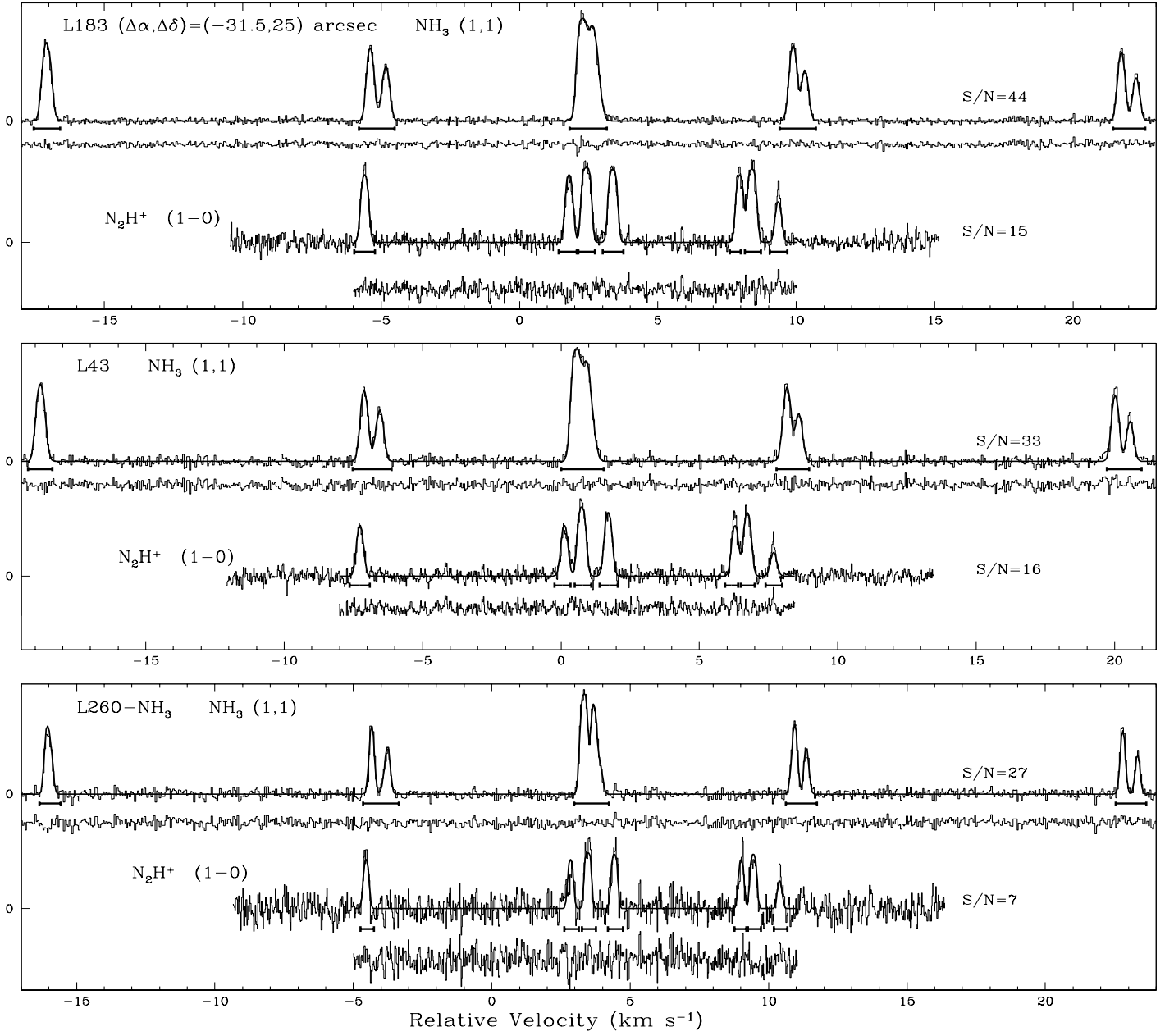


**Fig. 9.** Same as Fig. 7 but for the cores L183 (offset  $\Delta\alpha, \Delta\delta = -31.5, 25$  arcsec), L43, and L260-NH<sub>3</sub>.

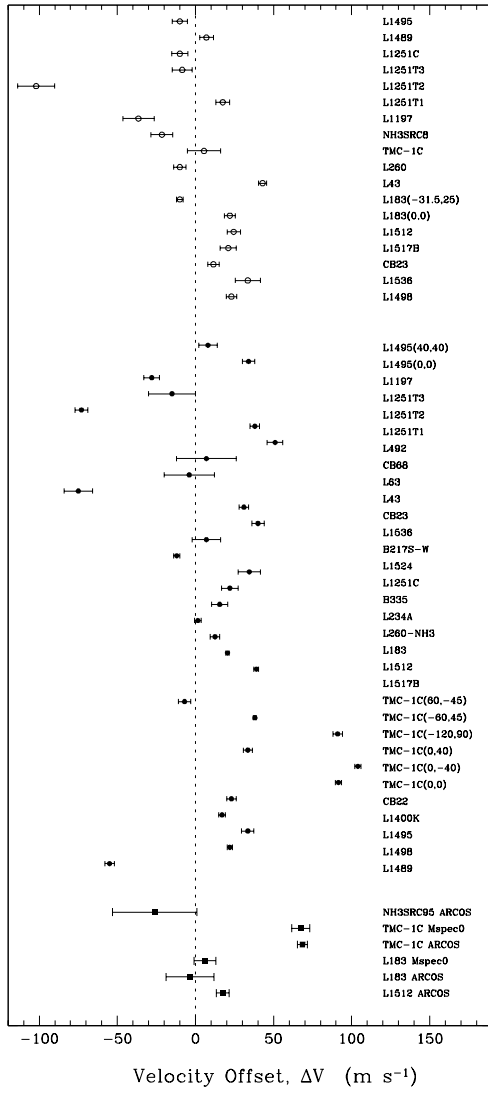


**Fig. 10.** Doppler velocity differences,  $\Delta V$ , between the  $\text{HC}_3\text{N } J = 2 - 1$  and  $\text{NH}_3 (J, K) = (1, 1)$  transitions for the data obtained at the 32-m (filled squares) and the 100-m (filled circles) telescopes, and between the  $\text{N}_2\text{H}^+ J = 1 - 0$  and  $\text{NH}_3 (J, K) = (1, 1)$  transitions for the 45-m telescope data (open circles). The  $1\sigma$  statistical errors are indicated. Given in parentheses are the coordinate offsets in arcsec.

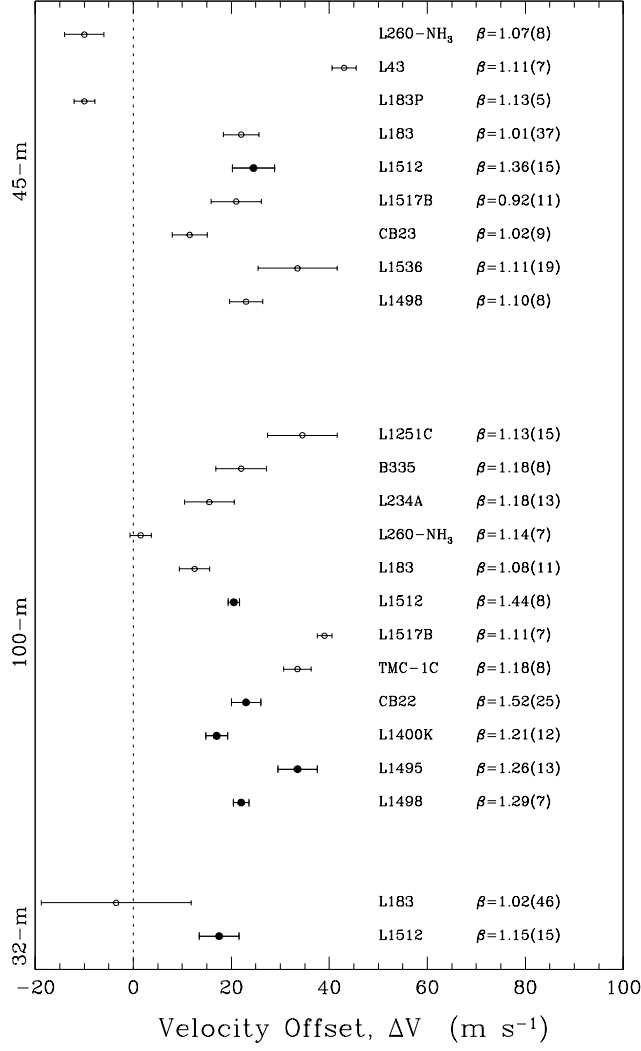


**Fig. 11.** Doppler velocity differences,  $\Delta V$ , between the  $\text{HC}_3\text{N } J = 2 - 1$  and  $\text{NH}_3 (J, K) = (1, 1)$  transitions for the data obtained at the 32-m and 100-m telescopes, and between the  $\text{N}_2\text{H}^+ J = 1 - 0$  and  $\text{NH}_3 (J, K) = (1, 1)$  transitions for the 45-m telescope data ( $1\sigma$  statistical errors are indicated). The parameter  $\beta$  is the ratio of the Doppler  $b$ -parameters:  $\beta = b(\text{NH}_3)/b(\text{HC}_3\text{N})$ , or  $\beta = b(\text{NH}_3)/b(\text{N}_2\text{H}^+)$ . Given in parentheses are  $1\sigma$  errors. The filled circles mark sources with thermally dominated motions.

**Table 5.** Radial velocities,  $V_{lsr}$ , Doppler parameters,  $b$ , and corresponding  $\chi^2_\nu$  values normalized per degree of freedom. Data from the Medicina 32-m and Effelsberg 100-m radio telescopes. The numbers in parentheses correspond to  $1\sigma$  statistical errors.

Object	$V_{lsr}, \text{ km s}^{-1} / b, \text{ km s}^{-1} / \chi^2_\nu$					HC <sub>3</sub> N (2 – 1)		$\Delta V$ ( $\text{m s}^{-1}$ )
	NH <sub>3</sub> (1,1)		central	total	low	high	total	
	outer	inner						
<i>Medicina 32-m radio telescope</i>								
L1512	7.0800(60) 0.1299(93) 1.04	7.0795(47) 0.116(18) 0.89	7.0760(41) 0.1138(51) 0.38	7.0790(28) 0.1189(47) 0.89		7.0965(30) 0.1037(96) 0.78		+17.5(4.1)
L183	2.4000(63) 0.129(18) 1.16	2.3970(49) 0.148(13) 0.88	2.4140(60) 0.1297(55) 0.74	2.4075(32) 0.1363(51) 1.30		2.404(15) 0.134(61) 0.97		-3.5(15.3)
<i>Effelsberg 100-m radio telescope</i>								
L1498	7.8025(16) 0.1125(31) 1.64	7.8080(13) 0.1138(64) 0.87	7.8065(13) 0.1227(14) 0.80	7.8060(8) 0.1177(13) 1.22	7.8290(38) 0.105(13) 1.19	7.8280(15) 0.0904(52) 0.55	7.8280(14) 0.0910(48) 0.99	+22.0(1.6)
L1495	6.7690(30) 0.1421(57) 1.36	6.7830(27) 0.147(17) 0.69	6.7895(19) 0.1425(20) 0.87	6.7840(14) 0.1446(19) 1.09		6.8175(38) 0.113(14) 0.86	6.8175(37) 0.115(12) 0.89	+33.5(4.0)
L1400K	3.2580(28) 0.1277(50) 1.40	3.2555(21) 0.1111(59) 1.00	3.2650(19) 0.1224(24) 0.88	3.2600(13) 0.1165(20) 1.18	3.2690(50) 0.107(16) 0.52	3.2780(20) 0.0986(96) 0.70	3.2770(18) 0.0961(94) 1.0	+17.0(2.2)
CB22	5.9665(26) 0.1256(60) 1.10	5.9675(20) 0.125(11) 0.89	5.9740(17) 0.1357(19) 0.75	5.9705(11) 0.1305(18) 1.02		5.9945(30) 0.088(17) 0.44	5.9935(28) 0.086(14) 1.02	+23.0(3.0)
TMC-1C <sup>a</sup>	5.2405(36) 0.0997(70) 1.17	5.2570(36) 0.126(10) 0.85	5.2575(28) 0.1135(32) 0.43	5.2540(19) 0.1213(29) 0.94	5.2815(56) 0.086(24) 0.75	5.2880(22) 0.1055(70) 1.11	5.2875(20) 0.1032(66) 0.92	+33.5(2.8)
L1517B	5.7800(20) 0.1131(40) 1.18	5.7830(17) 0.1229(61) 0.79	5.7855(18) 0.1201(17) 0.55	5.7835(10) 0.1216(16) 0.96	5.8200(76) 0.126(60) 0.91	5.8250(23) 0.1073(69) 0.70	5.8245(20) 0.1100(68) 0.82	+39.0(1.5)
L1512	7.1165(24) 0.1244(35) 1.30	7.1120(13) 0.1166(62) 0.76	7.1130(13) 0.1135(15) 0.77	7.1130(8) 0.1132(13) 1.03		7.1345(9) 0.0784(43) 0.94	7.1335(9) 0.0786(41) 1.04	+20.5(1.2)
L183	2.4200(13) 0.1062(25) 1.14	2.4170(11) 0.1149(40) 0.75	2.4220(12) 0.1166(13) 0.54	2.4195(7) 0.1118(11) 0.98		2.4335(32) 0.097(18) 0.71	2.4320(30) 0.104(11) 1.00	+12.5(3.1)
L260-NH <sub>3</sub>	3.4605(15) 0.1089(30) 1.58	3.4635(11) 0.1082(39) 0.93	3.4580(15) 0.1126(15) 1.16	3.4615(8) 0.1084(13) 1.39	3.4565(50) 0.084(14) 1.26	3.4645(21) 0.0973(72) 0.84	3.4630(20) 0.0951(61) 1.15	+1.5(2.2)
L234A	2.8935(50) 0.1337(93) 0.98	2.9065(57) 0.170(45) 0.73	2.9030(35) 0.1601(33) 0.83	2.9030(25) 0.1596(32) 0.90		2.9165(40) 0.136(14) 0.92	2.9185(45) 0.135(15) 0.73	+15.5(5.1)
B335	8.3350(25) 0.2312(55) 0.84	8.3430(27) 0.2326(36) 1.29	8.3250(20) 0.2138(22) 0.89	8.3365(14) 0.2294(19) 1.14		8.3545(51) 0.196(12) 0.61	8.3585(50) 0.195(13) 0.99	+22.0(5.2)
L1251C	-4.7390(22) 0.1396(55) 1.77	-4.7360(21) 0.1614(64) 1.18	-4.7200(21) 0.1577(21) 0.67	-4.7320(12) 0.1588(18) 1.48		-4.7005(70) 0.146(18) 0.65	-4.6975(70) 0.141(19) 0.74	+34.5(7.1)

<sup>a</sup> Offset  $(\Delta\alpha, \Delta\delta) = (0'', 40'')$ .

**Table 6.** Radial velocities,  $V_{lsr}$ , Doppler parameters,  $b$ , and corresponding  $\chi^2_\nu$  values normalized per degree of freedom. Data from the Nobeyama 45-m radio telescope. The numbers in parentheses correspond to  $1\sigma$  statistical errors.

Object	$V_{lsr}, \text{ km s}^{-1} / b, \text{ km s}^{-1} / \chi^2_\nu$							$\Delta V$ ( $\text{m s}^{-1}$ )
	NH <sub>3</sub> (1,1)			N <sub>2</sub> H <sup>+</sup> (1 – 0)				
	outer	inner	central	total	low	high	total	
L1498	7.8215(30) 0.1080(54) 1.37	7.8210(25) 0.116(11) 0.65	7.8180(25) 0.1129(30) 1.07	7.8200(15) 0.1124(26) 1.00	7.8450(42) 0.092(15) 0.84	7.8400(43) 0.0987(40) 1.16	7.8430(30) 0.1025(68) 1.08	+23.0(3.4)
L1536	5.5900(28) 0.1284(66) 0.90	5.5935(24) 0.1306(94) 1.16	5.6030(27) 0.1391(27) 1.07	5.5955(15) 0.1315(26) 1.15	5.629(11) 0.121(24) 0.76	5.6295(92) 0.117(40) 0.77	5.6290(80) 0.118(20) 0.75	+33.5(8.1)
CB23	6.0345(30) 0.1027(65) 1.47	6.0365(22) 0.106(11) 0.84	6.0325(22) 0.1071(28) 0.86	6.0345(14) 0.1064(25) 1.08	6.0515(46) 0.097(13) 0.64	6.0385(45) 0.119(12) 1.40	6.0460(33) 0.1043(92) 1.00	+11.5(3.6)
L1517B	5.8015(62) 0.107(12) 1.13	5.7980(60) 0.119(28) 0.45	5.7965(58) 0.1228(64) 1.15	5.7985(34) 0.1171(57) 0.84	5.8190(50) 0.109(21) 1.00	5.8215(53) 0.138(16) 1.03	5.8195(38) 0.127(14) 1.03	+21.0(5.1)
L1512	7.0925(59) 0.127(14) 0.59	7.1030(38) 0.112(21) 0.93	7.1080(42) 0.1210(48) 1.00	7.1025(25) 0.1158(43) 0.94	7.1290(45) 0.0847(92) 0.89	7.1260(41) 0.085(11) 0.89	7.1270(35) 0.0850(90) 0.86	+24.5(4.3)
L183	2.4195(27) 0.1490(78) 1.55	2.4165(26) 0.1563(65) 1.01	2.4275(33) 0.1536(29) 1.75	2.4225(16) 0.1563(27) 1.64	2.4395(50) 0.149(17) 0.91	2.4485(45) 0.1484(61) 0.82	2.4445(32) 0.154(56) 0.91	+22.0(3.6)
L183 <sup>a</sup>	2.4245(19) 0.1579(50) 1.18	2.4265(18) 0.1681(45) 0.82	2.4375(27) 0.1816(22) 1.32	2.4265(11) 0.1610(20) 1.43	2.4190(26) 0.1325(64) 1.18	2.4135(26) 0.1624(69) 1.01	2.4165(18) 0.1423(54) 1.30	−10.0(2.1)
L43	0.7020(25) 0.1523(63) 1.46	0.7040(27) 0.1748(64) 1.37	0.7150(27) 0.1859(29) 0.84	0.7050(16) 0.1677(25) 1.43	0.7485(31) 0.1368(88) 1.81	0.7470(25) 0.173(17) 0.90	0.7480(19) 0.1512(93) 1.60	+43.0(2.5)
L260-NH <sub>3</sub>	3.4815(25) 0.1053(55) 1.26	3.4800(21) 0.119(10) 0.83	3.4750(25) 0.1144(26) 0.53	3.4790(14) 0.1131(23) 1.06	3.4700(59) 0.0997(82) 1.34	3.4710(52) 0.111(26) 1.12	3.4690(37) 0.1061(79) 1.24	−10.0(4.0)

<sup>a</sup> Offset  $(\Delta\alpha, \Delta\delta) = (-31.5'', 25'')$ .